

Energy-conserving 3D elastic wave simulation with finite difference discretization on staggered grids with nonconforming interfaces

Longfei Gao¹, Omar Ghattas², and David Keyes³

¹ *Oden Institute for Computational Engineering and Sciences, The University of Texas at Austin, Austin, TX 78712, USA. E-mail: longfei.gao@austin.utexas.edu*

² *Oden Institute for Computational Engineering and Sciences, Jackson School of Geosciences, and Department of Mechanical Engineering, The University of Texas at Austin, Austin, TX 78712, USA*

³ *Division of Computer, Electrical and Mathematical Sciences and Engineering, King Abdullah University of Science and Technology, Thuwal 23955-6900, Saudi Arabia*

SUMMARY

In this work, we describe an approach to stably simulate the 3D isotropic elastic wave propagation using finite difference discretization on staggered grids with nonconforming interfaces. Specifically, we consider simulation domains composed of layers of uniform grids with different grid spacings, separated by planar interfaces. This discretization setting is motivated by the observation that wave speeds of earth media tend to increase with depth due to sedimentation and consolidation processes. We demonstrate that the layer-wise finite difference discretization approach has the potential to significantly reduce the simulation cost, compared to its counterpart that uses holistically uniform grids. Such discretizations are enabled by summation-by-parts finite difference operators, which are standard finite difference operators with special adaptations near boundaries or interfaces, and simultaneous approxi-

mation terms, which are penalty terms appended to the discretized system to weakly impose boundary or interface conditions. Combined with specially designed interpolation operators, the discretized system is shown to preserve the energy-conserving property of the continuous elastic wave equation, and *a fortiori* ensure the stability of the simulation. Numerical examples are presented to corroborate these analytical developments.

Key words: Numerical modelling; Wave propagation; Computational seismology.

1 INTRODUCTION

We aim to discretize the 3D isotropic elastic wave equation on layer-wise uniform grids as illustrated in Fig. 1, where the entire simulation domain is separated into individual layers, each discretized with uniform grids of different spatial grid spacings. This discretization setting is motivated by the observation that wave speeds of earth media tend to increase with depth due to sedimentation and consolidation processes. For instance, soil and dry sand on earth's surface can have shear wave speeds as low as 100 m/s while hard rocks in deeper part of the earth can have shear wave speeds above 3000 m/s and compressional wave speeds around 6000 m/s (see, e.g., Bourbié et al. 1987, p. 240).

For fixed frequency, wavelengths of the seismic waves are proportional to the wave speeds associated with the subterranean media through which they propagate. The spatial grid spacing in a wave simulation is usually dictated by the minimal wavelength of the propagating waves, and hence is determined by the minimal wave speed of the media. Moreover, the temporal step size in a wave simulation is usually constrained by the spatial grid spacing and the maximal wave speed of the medium through the Courant-Friedrichs-Lewy (CFL) stability condition. An illustrative thought experiment is presented in Appendix A to meticulously demonstrate the impact of wave speed variation on discretization parameters. In brief, compared to addressing a simulation domain composed of different subterranean media with a holistically uniform spatial discretization grid, using a layer-wise uniform spatial discretization grid can significantly reduce the expenditure in computational resources.

Fully unstructured finite element based discretizations can address the variation in wave speed by allowing variation in the sizes of the individual elements. Such an approach has been thoroughly investigated in previous works; see Lysmer & Drake (1972); Bao et al. (1998); Komatitsch & Vilotte (1998); Komatitsch & Tromp (1999, 2002); Chaljub et al. (2003, 2007);

Käser & Dumbser (2006); Dumbser & Käser (2006); Etienne et al. (2010); Wilcox et al. (2010); Peter et al. (2011); Bui-Thanh & Ghattas (2012), for example. However, these discretizations tend to be more complex to implement and more expensive to compute than those using finite differences on a per grid point basis. For earth media, at least at the exploration scale, finite difference discretizations on layer-wise uniform grids seem to be an attractive compromise between the expensive fully unstructured finite element schemes and the wasteful holistically uniform finite difference schemes. Previous work adopting this approach can be found in, e.g., Hayashi et al. (2001); Kristek et al. (2010); Zhang et al. (2013); Nie et al. (2017); Gao et al. (2018) and the references therein. However, these earlier attempts are often affected by the instability issue associated with the nonconforming interface.

In this work, we follow up our previous 2D study in Gao & Keyes (2020b) and make use of the summation by parts (SBP)-simultaneous approximation terms (SATs) technique to address the nonconforming interface. This technique is guided by energy analysis to construct stable spatial discretizations. The concept of SBP finite difference operators dates back to Kreiss & Scherer (1974), which adapts standard finite difference operators near boundaries or interfaces to mimic the integration-by-parts property in the continuous operators of the partial differential equations. The concept of SATs dates back to Carpenter et al. (1994), which appends penalty terms (i.e., SATs) to the discretized system to weakly impose boundary or interface conditions. Other related work on the SBP-SAT technique can be found in Strand (1994); Hicken & Zingg (2013); Fernández et al. (2014); Svärd & Nordström (2014); Kozdon & Wilcox (2016); Wang et al. (2016); Prochnow et al. (2017); Mattsson & O’Reilly (2018); Gao et al. (2019); Gao & Keyes (2019, 2020a), among others.

Applied to the layer-wise discretization setting considered in this work, the individual layers are first discretized independently using SBP finite difference operators and then combined together through SATs. An important component of the SATs is the compatible interpolation operators that transfer data at the layer interfaces. A collection of such interpolation operators corresponding to a variety of grid spacing ratios is presented in Appendix B. The grid spacing ratios are allowed to be fractional numbers, instead of merely integers, which improves the application flexibility of the proposed discretization setting. With carefully designed SBP operators, SATs, and interpolation operators, the resulting spatial discretization preserves the energy-conserving property of the continuous elastic wave equation, and *a fortiori* ensures the stability of the simulation.

Such a discretization procedure bears a similarity with the discontinuous Galerkin (DG) method in the sense that an entire layer can be viewed as the analogue of an element in the DG

method, while the SATs resemble the numerical fluxes in the DG method; see (Hesthaven & Warburton 2008, p. 13). However, the ‘discontinuity’ of discretization in the proposed method occurs at a much coarser granular level than in the DG method.

In the rest of this paper, we first formulate the underlying problem in Section 2. Methodology of the proposed discretization is presented in Section 3, followed by numerical demonstrations in Section 4. Finally, conclusions are drawn in Section 5.

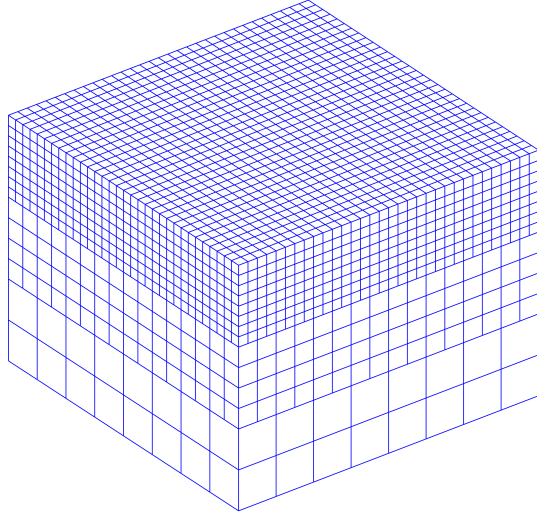


Figure 1: Illustration of the layer-wise uniform grid discretization setting. Each individual layer is discretized uniformly. Different layers are discretized using different grid spacings.

2 PROBLEM DESCRIPTION

Omitting the external source terms, the elastic wave propagation can be described using the following velocity-stress formulation:

$$\begin{cases} \rho \dot{v}_i = \sigma_{ij,j}; & (1a) \\ \dot{\sigma}_{ij} = C_{ijkl} \left(\frac{v_{k,l} + v_{l,k}}{2} \right), & (1b) \end{cases}$$

where the Einstein summation convention applies to subscript indices. In eq. (1), v_i and σ_{ij} are the sought solution variables, standing for components of the velocity vector and the stress tensor, respectively; ρ and C_{ijkl} are given physical parameters, standing for density and components of the stiffness tensor, respectively. In the case of isotropic media, eq. (1b) can be written as

$$\dot{\sigma}_{ij} = \lambda \delta_{ij} v_{k,k} + \mu (v_{i,j} + v_{j,i}), \quad (2)$$

where λ and μ are the Lamé parameters, while δ_{ij} stands for the Kronecker delta.

The above equations can also be expressed in the following form:

$$\left\{ \begin{array}{l} \frac{\partial v_x}{\partial t} = \frac{1}{\rho} \left(\frac{\partial \sigma_{xx}}{\partial x} + \frac{\partial \sigma_{xy}}{\partial y} + \frac{\partial \sigma_{xz}}{\partial z} \right); \quad (3a) \\ \frac{\partial v_y}{\partial t} = \frac{1}{\rho} \left(\frac{\partial \sigma_{xy}}{\partial x} + \frac{\partial \sigma_{yy}}{\partial y} + \frac{\partial \sigma_{yz}}{\partial z} \right); \quad (3b) \\ \frac{\partial v_z}{\partial t} = \frac{1}{\rho} \left(\frac{\partial \sigma_{xz}}{\partial x} + \frac{\partial \sigma_{yz}}{\partial y} + \frac{\partial \sigma_{zz}}{\partial z} \right); \quad (3c) \\ \frac{\partial \sigma_{xx}}{\partial t} = (\lambda + 2\mu) \frac{\partial v_x}{\partial x} + \lambda \frac{\partial v_y}{\partial y} + \lambda \frac{\partial v_z}{\partial z}; \quad (3d) \\ \frac{\partial \sigma_{yy}}{\partial t} = \lambda \frac{\partial v_x}{\partial x} + (\lambda + 2\mu) \frac{\partial v_y}{\partial y} + \lambda \frac{\partial v_z}{\partial z}; \quad (3e) \\ \frac{\partial \sigma_{zz}}{\partial t} = \lambda \frac{\partial v_x}{\partial x} + \lambda \frac{\partial v_y}{\partial y} + (\lambda + 2\mu) \frac{\partial v_z}{\partial z}; \quad (3f) \\ \frac{\partial \sigma_{xy}}{\partial t} = \mu \left(\frac{\partial v_y}{\partial x} + \frac{\partial v_x}{\partial y} \right); \quad (3g) \\ \frac{\partial \sigma_{yz}}{\partial t} = \mu \left(\frac{\partial v_z}{\partial y} + \frac{\partial v_y}{\partial z} \right); \quad (3h) \\ \frac{\partial \sigma_{xz}}{\partial t} = \mu \left(\frac{\partial v_x}{\partial z} + \frac{\partial v_z}{\partial x} \right), \quad (3i) \end{array} \right.$$

which is cumbersome for the ensuing discussion, but convenient for implementation on computers.

Within each layer, the spatial discretization is carried out on the standard staggered grids (see, e.g., Yee 1966; Virieux 1986; Levander 1988), whose layout are depicted in Fig. 2. Specifically, the three normal stress components together occupy one grid, while each shear stress component and each velocity component occupies one grid.

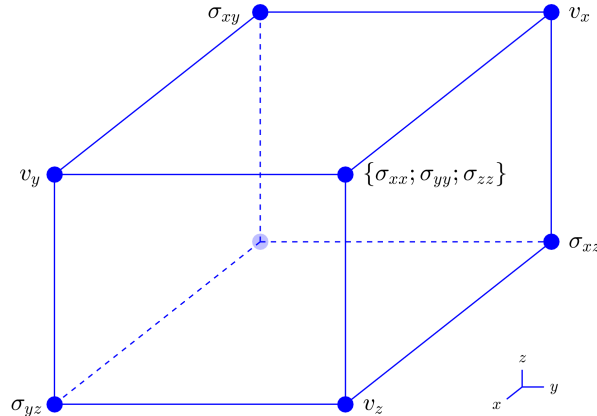


Figure 2: Illustration of the grid staggering.

3 METHODOLOGY

3.1 SBP operators on 1D staggered grids

To motivate the concept of SBP operators, let us briefly consider the case of 1D wave propagation on staggered grids. We note here that similar 1D presentation has already appeared in previous works (e.g., Gao et al. 2019). It is recapitulated here to make this work self-contained. Specifically, the 1D wave propagation can be described by the following system:

$$\begin{cases} \rho \frac{\partial v}{\partial t} = \frac{\partial \sigma}{\partial x}; & (4a) \\ \beta \frac{\partial \sigma}{\partial t} = \frac{\partial v}{\partial x}, & (4b) \end{cases}$$

where $\beta = \frac{1}{\rho c^2}$ stands for compressibility.

Supposing the above wave system is defined over interval (x_L, x_R) , its associated physical energy can be expressed as:

$$\mathcal{E} = \frac{1}{2} \int_{x_L}^{x_R} (\rho v^2 + \beta \sigma^2) dx. \quad (5)$$

Taking the time derivative of eq. (5), substituting the equations from (4), and applying the integration-by-parts formula, we arrive at:

$$\frac{d\mathcal{E}}{dt} = -\sigma(x_L) \cdot v(x_L) + \sigma(x_R) \cdot v(x_R). \quad (6)$$

In other words, time derivative of the physical energy \mathcal{E} reduces to boundary data only. If free surface boundary condition is associated with both boundaries, i.e., $\sigma(x_L) = \sigma(x_R) = 0$, we have that $\frac{d\mathcal{E}}{dt} = 0$, i.e., the physical energy is conservative.

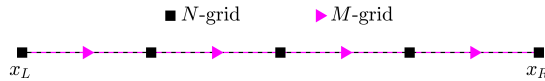


Figure 3: Illustration of a set of 1D staggered grids.

Supposing that wave system (4) is discretized on a set of staggered grids illustrated in Fig. 3 with σ occupying the N -grid, which includes the two boundary points, and v occupying the M -grid, which consists of only interior grid points, the semi-discretized system can be expressed as:

$$\begin{cases} \mathcal{A}^M \boldsymbol{\rho}^M \frac{dV}{dt} = \mathcal{A}^M \mathcal{D}^N \Sigma; & (7a) \\ \mathcal{A}^N \boldsymbol{\beta}^N \frac{d\Sigma}{dt} = \mathcal{A}^N \mathcal{D}^M V, & (7b) \end{cases}$$

where V and Σ are discretized solution vectors; diagonal matrices $\boldsymbol{\rho}^M$ and $\boldsymbol{\beta}^N$ are the discrete

correspondences of ρ and β in eq. (4), respectively; matrices \mathcal{D}^N and \mathcal{D}^M are finite difference operators approximating $\frac{\partial}{\partial x}$, which apply on vectors defined on the N - and M -grid, respectively; finally, diagonal matrices \mathcal{A}^M and \mathcal{A}^N are referred to as norm matrices, which are formally redundant in the above equations, but will play an important role in the upcoming discussion.

Analogous to eq. (5), the discrete energy associated with the above semi-discretized system is defined as:

$$E = \frac{1}{2}V^T(\mathcal{A}^M \boldsymbol{\rho}^M)V + \frac{1}{2}\Sigma^T(\mathcal{A}^N \boldsymbol{\beta}^N)\Sigma. \quad (8)$$

Taking the time derivative of eq. (8) and substituting the equations from (7), we arrive at:

$$\frac{dE}{dt} = \Sigma^T [\mathcal{A}^N \mathcal{D}^M + (\mathcal{A}^M \mathcal{D}^N)^T] V. \quad (9)$$

To simplify the notation, we introduce matrix Q , which is defined as

$$Q = \mathcal{A}^N \mathcal{D}^M + (\mathcal{A}^M \mathcal{D}^N)^T. \quad (10)$$

For eq. (9) to mimic eq. (6), we ask Q to satisfy the following property:

$$Q = -\mathcal{E}^L (\mathcal{P}^L)^T + \mathcal{E}^R (\mathcal{P}^R)^T, \quad (11)$$

where \mathcal{E}^L and \mathcal{E}^R are the canonical basis vectors whose first and last components are 1, respectively; \mathcal{P}^L and \mathcal{P}^R are projection operators that can be applied on vector V to provide approximations to $v(x_L)$ and $v(x_R)$, respectively.

With the above property, eq. (9) can be written as:

$$\frac{dE}{dt} = -(\mathcal{E}^L)^T \Sigma \cdot (\mathcal{P}^L)^T V + (\mathcal{E}^R)^T \Sigma \cdot (\mathcal{P}^R)^T V. \quad (12)$$

Realizing that $(\mathcal{E}^L)^T \Sigma$, $(\mathcal{P}^L)^T V$, $(\mathcal{E}^R)^T \Sigma$, and $(\mathcal{P}^R)^T V$ are approximations to $\sigma(x_L)$, $v(x_L)$, $\sigma(x_R)$, and $v(x_R)$, respectively, we have that the discrete energy E in eq. (9) mimics the behavior of \mathcal{E} in eq. (6).

The property of Q in eq. (11) is attained by carefully constructing the SBP operators \mathcal{A}^N , \mathcal{D}^M , \mathcal{A}^M , and \mathcal{D}^N appearing in its definition in eq. (10). In practice, such SBP operators are often constructed with the assistance from symbolic computing software. One may refer to (Gao et al. 2019, p. 6) for an example of such SBP operators, which will be used throughout this study. (We note here that the choice of SBP finite difference operators is not unique. For example, another possible choice can be found in O'Reilly et al. (2017).) The SBP operators from Gao et al. (2019) are included in Appendix C to make this work self-contained. From eq. (C.1), we can see that in the interior, the finite difference operators \mathcal{D}^M and \mathcal{D}^N are the

same as the standard fourth-order staggered grid stencil $[^{1/24}, -^{9/8}, ^{9/8}, -^{1/24}]/\Delta x$ from (Levander 1988), and that only the stencils near the boundaries are adapted.

The norm matrices \mathcal{A}^N and \mathcal{A}^M , seemingly redundant in eq. (7), introduce extra degrees of freedom to allow Q to have the desired property. They reduce to the grid spacing Δx in the interior and vary only near the boundaries. In the above energy analysis, \mathcal{A}^N and \mathcal{A}^M play the role of the integral operator $\int_{x_L}^{x_R}$ in eq. (5), and can be understood as providing the quadrature rules (see Hicken & Zingg 2013). In this work, we only consider the case where \mathcal{A}^N and \mathcal{A}^M are diagonal, so that products $(\mathcal{A}^M \boldsymbol{\rho}^M)$ and $(\mathcal{A}^N \boldsymbol{\beta}^N)$ are symmetric, and, consequently, the expression in eq. (8) provides a valid definition of discrete energy. A drawback of this choice of diagonal norm matrices is that the formal order of the stencils near the boundary can only be as high as half of that in the interior.

In the following, we use the terminology ‘discrete energy analysis’ to refer to the procedure of taking the time derivative of the discrete energy, substituting the semi-discretized system to replace the temporal derivatives of the solution variables, and finally, invoking the properties built in the SBP operators to reduce the result to boundaries or interfaces.

The free surface boundary conditions $\sigma(x_L) = \sigma(x_R) = 0$ can be imposed by appending penalty terms to eq. (7), leading to the following modified system:

$$\left\{ \begin{array}{l} \mathcal{A}^M \boldsymbol{\rho}^M \frac{dV}{dt} = \mathcal{A}^M \mathcal{D}^N \Sigma + \mathcal{P}^L [(\boldsymbol{\varepsilon}^L)^T \Sigma - \mathbf{0}] - \mathcal{P}^R [(\boldsymbol{\varepsilon}^R)^T \Sigma - \mathbf{0}] ; \\ \mathcal{A}^N \boldsymbol{\beta}^N \frac{d\Sigma}{dt} = \mathcal{A}^N \mathcal{D}^M V. \end{array} \right. \quad (13a)$$

$$\quad (13b)$$

Following the aforementioned procedure of discrete energy analysis, one can verify that the discrete energy E as defined in eq. (8) is conservative, i.e., $\frac{dE}{dt} = 0$, for the above modified system.

3.2 SBP finite difference operators on 3D staggered grids

The 1D SBP operators introduced above serve as the building blocks of the 3D SBP operators used in this work. We append subscripts x , y , and z to the 1D operators \mathcal{A}^N , \mathcal{D}^M , \mathcal{A}^M , and \mathcal{D}^N to distinguish the directions. By design, these 1D operators satisfy the following properties:

$$Q_x = \mathcal{A}_x^N \mathcal{D}_x^M + (\mathcal{A}_x^M \mathcal{D}_x^N)^T = -\boldsymbol{\varepsilon}_x^L (\mathcal{P}_x^L)^T + \boldsymbol{\varepsilon}_x^R (\mathcal{P}_x^R)^T, \quad (14a)$$

$$Q_y = \mathcal{A}_y^N \mathcal{D}_y^M + (\mathcal{A}_y^M \mathcal{D}_y^N)^T = -\boldsymbol{\varepsilon}_y^L (\mathcal{P}_y^L)^T + \boldsymbol{\varepsilon}_y^R (\mathcal{P}_y^R)^T, \quad (14b)$$

$$Q_z = \mathcal{A}_z^N \mathcal{D}_z^M + (\mathcal{A}_z^M \mathcal{D}_z^N)^T = -\boldsymbol{\varepsilon}_z^L (\mathcal{P}_z^L)^T + \boldsymbol{\varepsilon}_z^R (\mathcal{P}_z^R)^T. \quad (14c)$$

Furthermore, we use \mathcal{I}_x^N , \mathcal{I}_x^M , \mathcal{I}_y^N , \mathcal{I}_y^M , \mathcal{I}_z^N , and \mathcal{I}_z^M to denote the identity matrices corresponding to the N - and M -grids of the x -, y -, and z -directions, respectively.

The 3D norm matrices are constructed as the tensor products of the 1D norm matrices as follows:

$$\begin{aligned} \mathcal{A}^{V_x} &= \mathcal{A}_x^M \otimes \mathcal{A}_y^N \otimes \mathcal{A}_z^N, & \mathcal{A}^{\Sigma_{xy}} &= \mathcal{A}_x^M \otimes \mathcal{A}_y^M \otimes \mathcal{A}_z^N, & \mathcal{A}^{\Sigma_{xx}} &= \mathcal{A}_x^N \otimes \mathcal{A}_y^N \otimes \mathcal{A}_z^N, \\ \mathcal{A}^{V_y} &= \mathcal{A}_x^N \otimes \mathcal{A}_y^M \otimes \mathcal{A}_z^N, & \mathcal{A}^{\Sigma_{yz}} &= \mathcal{A}_x^N \otimes \mathcal{A}_y^M \otimes \mathcal{A}_z^M, & \mathcal{A}^{\Sigma_{yy}} &= \mathcal{A}_x^N \otimes \mathcal{A}_y^N \otimes \mathcal{A}_z^N, \\ \mathcal{A}^{V_z} &= \mathcal{A}_x^N \otimes \mathcal{A}_y^N \otimes \mathcal{A}_z^M, & \mathcal{A}^{\Sigma_{xz}} &= \mathcal{A}_x^M \otimes \mathcal{A}_y^N \otimes \mathcal{A}_z^M, & \mathcal{A}^{\Sigma_{zz}} &= \mathcal{A}_x^N \otimes \mathcal{A}_y^N \otimes \mathcal{A}_z^N. \end{aligned} \quad (15)$$

The 3D finite difference operators are constructed as the tensor products of the 1D finite difference operators and the 1D identity matrices as follows:

$$\begin{aligned} \mathcal{D}_x^{\Sigma_{xx}} &= \mathcal{D}_x^N \otimes \mathcal{I}_y^N \otimes \mathcal{I}_z^N, & \mathcal{D}_y^{\Sigma_{xy}} &= \mathcal{I}_x^M \otimes \mathcal{D}_y^M \otimes \mathcal{I}_z^N, & \mathcal{D}_z^{\Sigma_{xz}} &= \mathcal{I}_x^M \otimes \mathcal{I}_y^N \otimes \mathcal{D}_z^M, \\ \mathcal{D}_x^{\Sigma_{xy}} &= \mathcal{D}_x^M \otimes \mathcal{I}_y^M \otimes \mathcal{I}_z^N, & \mathcal{D}_y^{\Sigma_{yy}} &= \mathcal{I}_x^N \otimes \mathcal{D}_y^N \otimes \mathcal{I}_z^N, & \mathcal{D}_z^{\Sigma_{yz}} &= \mathcal{I}_x^N \otimes \mathcal{I}_y^M \otimes \mathcal{D}_z^M, \\ \mathcal{D}_x^{\Sigma_{xz}} &= \mathcal{D}_x^M \otimes \mathcal{I}_y^N \otimes \mathcal{I}_z^M, & \mathcal{D}_y^{\Sigma_{yz}} &= \mathcal{I}_x^N \otimes \mathcal{D}_y^M \otimes \mathcal{I}_z^M, & \mathcal{D}_z^{\Sigma_{zz}} &= \mathcal{I}_x^N \otimes \mathcal{I}_y^N \otimes \mathcal{D}_z^N, \\ \mathcal{D}_x^{V_x} &= \mathcal{D}_x^M \otimes \mathcal{I}_y^N \otimes \mathcal{I}_z^N, & \mathcal{D}_y^{V_x} &= \mathcal{I}_x^M \otimes \mathcal{D}_y^N \otimes \mathcal{I}_z^N, & \mathcal{D}_z^{V_x} &= \mathcal{I}_x^M \otimes \mathcal{I}_y^N \otimes \mathcal{D}_z^N, \\ \mathcal{D}_x^{V_y} &= \mathcal{D}_x^N \otimes \mathcal{I}_y^M \otimes \mathcal{I}_z^N, & \mathcal{D}_y^{V_y} &= \mathcal{I}_x^N \otimes \mathcal{D}_y^M \otimes \mathcal{I}_z^N, & \mathcal{D}_z^{V_y} &= \mathcal{I}_x^N \otimes \mathcal{I}_y^M \otimes \mathcal{D}_z^N, \\ \mathcal{D}_x^{V_z} &= \mathcal{D}_x^N \otimes \mathcal{I}_y^N \otimes \mathcal{I}_z^M, & \mathcal{D}_y^{V_z} &= \mathcal{I}_x^N \otimes \mathcal{D}_y^N \otimes \mathcal{I}_z^M, & \mathcal{D}_z^{V_z} &= \mathcal{I}_x^N \otimes \mathcal{I}_y^N \otimes \mathcal{D}_z^M. \end{aligned} \quad (16)$$

Supposing that the 3D wave system described in eq. (1) is defined over a cuboid $\Omega = (x_L, x_R) \times (y_L, y_R) \times (z_L, z_R)$, its associated physical energy can be expressed as:

$$\mathcal{E} = \frac{1}{2} \int_{\Omega} (\rho v_i v_i + \sigma_{ij} S_{ijkl} \sigma_{kl}) d\Omega, \quad (17)$$

where S stands for the compliance tensor, which is the inverse of the stiffness tensor C from eq. (1b). Taking the time derivative of eq. (17), substituting the equations from (1), and applying the divergence theorem, we arrive at

$$\frac{d\mathcal{E}}{dt} = \int_{\partial\Omega} v_i \sigma_{ij} n_j d\partial\Omega, \quad (18)$$

where n_j stands for component of the outward normal vector on the boundary. From eq. (18), we have that the time derivative of the physical energy \mathcal{E} reduces to boundary data only, analogous to the 1D case as in eq. (6).

Replacing the spatial derivatives in eq. (1) with the 3D SBP operators introduced above, the resulting discretized system can be expressed as:

$$\begin{cases} \mathcal{A}^{V_i} \rho^{V_i} \frac{dV_i}{dt} = \mathcal{A}^{V_i} \mathcal{D}_j^{\Sigma_{ij}} \Sigma_{ij}; \end{cases} \quad (19a)$$

$$\begin{cases} \mathcal{A}^{\Sigma_{ij}} \mathcal{S}_{ijkl}^{\Sigma_{ij}} \frac{d\Sigma_{kl}}{dt} = \mathcal{A}^{\Sigma_{ij}} \frac{1}{2} \left(\mathcal{D}_j^{V_i} V_i + \mathcal{D}_i^{V_j} V_j \right), \end{cases} \quad (19b)$$

where the Einstein summation convention applies to subscript indices only (e.g., for the expression $\mathcal{A}^{V_i} \mathcal{D}_j^{\Sigma_{ij}} \Sigma_{ij}$ on the right hand side of eq. (19a), only the index j is summed over).

The discrete energy associated with eq. (19) is defined as

$$E = \frac{1}{2} V_i^T (\mathcal{A}^{V_i} \rho^{V_i}) V_i + \frac{1}{2} \Sigma_{ij}^T \left(\mathcal{A}^{\Sigma_{ij}} \mathbf{S}_{ijkl}^{\Sigma_{ij}} \right) \Sigma_{kl}. \quad (20)$$

Following the procedure of discrete energy analysis introduced in the previous section, it can be shown that

$$\begin{aligned} \frac{dE}{dt} = & - \left[\Sigma_{xx}^T (\mathcal{E}_x^L \otimes \mathcal{I}_y^N \otimes \mathcal{I}_z^N) \right] \cdot [\mathcal{A}_y^N \otimes \mathcal{A}_z^N] \cdot [(\mathcal{P}_x^L \otimes \mathcal{I}_y^N \otimes \mathcal{I}_z^N)^T V_x] \\ & + \left[\Sigma_{xx}^T (\mathcal{E}_x^R \otimes \mathcal{I}_y^N \otimes \mathcal{I}_z^N) \right] \cdot [\mathcal{A}_y^N \otimes \mathcal{A}_z^N] \cdot [(\mathcal{P}_x^R \otimes \mathcal{I}_y^N \otimes \mathcal{I}_z^N)^T V_x] \\ & - \left[\Sigma_{xy}^T (\mathcal{P}_x^L \otimes \mathcal{I}_y^M \otimes \mathcal{I}_z^N) \right] \cdot [\mathcal{A}_y^M \otimes \mathcal{A}_z^N] \cdot [(\mathcal{E}_x^L \otimes \mathcal{I}_y^M \otimes \mathcal{I}_z^N)^T V_y] \\ & + \left[\Sigma_{xy}^T (\mathcal{P}_x^R \otimes \mathcal{I}_y^M \otimes \mathcal{I}_z^N) \right] \cdot [\mathcal{A}_y^M \otimes \mathcal{A}_z^N] \cdot [(\mathcal{E}_x^R \otimes \mathcal{I}_y^M \otimes \mathcal{I}_z^N)^T V_y] \\ & - \left[\Sigma_{xz}^T (\mathcal{P}_x^L \otimes \mathcal{I}_y^N \otimes \mathcal{I}_z^M) \right] \cdot [\mathcal{A}_y^N \otimes \mathcal{A}_z^M] \cdot [(\mathcal{E}_x^L \otimes \mathcal{I}_y^N \otimes \mathcal{I}_z^M)^T V_z] \\ & + \left[\Sigma_{xz}^T (\mathcal{P}_x^R \otimes \mathcal{I}_y^N \otimes \mathcal{I}_z^M) \right] \cdot [\mathcal{A}_y^N \otimes \mathcal{A}_z^M] \cdot [(\mathcal{E}_x^R \otimes \mathcal{I}_y^N \otimes \mathcal{I}_z^M)^T V_z] \\ & - \left[\Sigma_{xy}^T (\mathcal{I}_x^M \otimes \mathcal{P}_y^L \otimes \mathcal{I}_z^N) \right] \cdot [\mathcal{A}_x^M \otimes \mathcal{A}_z^N] \cdot [(\mathcal{I}_x^M \otimes \mathcal{E}_y^L \otimes \mathcal{I}_z^N)^T V_x] \\ & + \left[\Sigma_{xy}^T (\mathcal{I}_x^M \otimes \mathcal{P}_y^R \otimes \mathcal{I}_z^N) \right] \cdot [\mathcal{A}_x^M \otimes \mathcal{A}_z^N] \cdot [(\mathcal{I}_x^M \otimes \mathcal{E}_y^R \otimes \mathcal{I}_z^N)^T V_x] \\ & - \left[\Sigma_{yy}^T (\mathcal{I}_x^N \otimes \mathcal{E}_y^L \otimes \mathcal{I}_z^N) \right] \cdot [\mathcal{A}_x^N \otimes \mathcal{A}_z^N] \cdot [(\mathcal{I}_x^N \otimes \mathcal{P}_y^L \otimes \mathcal{I}_z^N)^T V_y] \\ & + \left[\Sigma_{yy}^T (\mathcal{I}_x^N \otimes \mathcal{E}_y^R \otimes \mathcal{I}_z^N) \right] \cdot [\mathcal{A}_x^N \otimes \mathcal{A}_z^N] \cdot [(\mathcal{I}_x^N \otimes \mathcal{P}_y^R \otimes \mathcal{I}_z^N)^T V_y] \\ & - \left[\Sigma_{yz}^T (\mathcal{I}_x^N \otimes \mathcal{P}_y^L \otimes \mathcal{I}_z^M) \right] \cdot [\mathcal{A}_x^N \otimes \mathcal{A}_z^M] \cdot [(\mathcal{I}_x^N \otimes \mathcal{E}_y^L \otimes \mathcal{I}_z^M)^T V_z] \\ & + \left[\Sigma_{yz}^T (\mathcal{I}_x^N \otimes \mathcal{P}_y^R \otimes \mathcal{I}_z^M) \right] \cdot [\mathcal{A}_x^N \otimes \mathcal{A}_z^M] \cdot [(\mathcal{I}_x^N \otimes \mathcal{E}_y^R \otimes \mathcal{I}_z^M)^T V_z] \\ & - \left[\Sigma_{xz}^T (\mathcal{I}_x^M \otimes \mathcal{I}_y^N \otimes \mathcal{P}_z^L) \right] \cdot [\mathcal{A}_x^M \otimes \mathcal{A}_y^N] \cdot [(\mathcal{I}_x^M \otimes \mathcal{I}_y^N \otimes \mathcal{E}_z^L)^T V_x] \\ & + \left[\Sigma_{xz}^T (\mathcal{I}_x^M \otimes \mathcal{I}_y^N \otimes \mathcal{P}_z^R) \right] \cdot [\mathcal{A}_x^M \otimes \mathcal{A}_y^N] \cdot [(\mathcal{I}_x^M \otimes \mathcal{I}_y^N \otimes \mathcal{E}_z^R)^T V_x] \\ & - \left[\Sigma_{yz}^T (\mathcal{I}_x^N \otimes \mathcal{I}_y^M \otimes \mathcal{P}_z^L) \right] \cdot [\mathcal{A}_x^N \otimes \mathcal{A}_y^M] \cdot [(\mathcal{I}_x^N \otimes \mathcal{I}_y^M \otimes \mathcal{E}_z^L)^T V_y] \\ & + \left[\Sigma_{yz}^T (\mathcal{I}_x^N \otimes \mathcal{I}_y^M \otimes \mathcal{P}_z^R) \right] \cdot [\mathcal{A}_x^N \otimes \mathcal{A}_y^M] \cdot [(\mathcal{I}_x^N \otimes \mathcal{I}_y^M \otimes \mathcal{E}_z^R)^T V_y] \\ & - \left[\Sigma_{zz}^T (\mathcal{I}_x^N \otimes \mathcal{I}_y^N \otimes \mathcal{E}_z^L) \right] \cdot [\mathcal{A}_x^N \otimes \mathcal{A}_y^N] \cdot [(\mathcal{I}_x^N \otimes \mathcal{I}_y^N \otimes \mathcal{P}_z^L)^T V_z] \\ & + \left[\Sigma_{zz}^T (\mathcal{I}_x^N \otimes \mathcal{I}_y^N \otimes \mathcal{E}_z^R) \right] \cdot [\mathcal{A}_x^N \otimes \mathcal{A}_y^N] \cdot [(\mathcal{I}_x^N \otimes \mathcal{I}_y^N \otimes \mathcal{P}_z^R)^T V_z] \end{aligned} \quad \left. \begin{array}{l} \text{\textit{yz-faces}} \\ \text{\textit{xz-faces}} \\ \text{\textit{xy-faces,}} \end{array} \right\} \quad (21)$$

which again reduces to boundary data only. In order to see this more clearly, let us take the first line of eq. (21) as an example. Recognizing that $[\Sigma_{xx}^T (\mathcal{E}_x^L \otimes \mathcal{I}_y^N \otimes \mathcal{I}_z^N)]$ is the restriction of Σ_{xx} on the yz -face at $x = x_L$, while $[(\mathcal{P}_x^L \otimes \mathcal{I}_y^N \otimes \mathcal{I}_z^N)^T V_x]$ is the projection of V_x on the

same face, we have that the expression in this line is an approximation to

$$- \int_{y_L}^{y_R} \int_{z_L}^{z_R} \sigma_{xx}(x_L, y, z) v_x(x_L, y, z) dydz, \quad (22)$$

with $[\mathcal{A}_y^N \otimes \mathcal{A}_z^N]$ playing the role of the integral operators in eq. (22). Similar interpretations apply to the other lines of eq. (21). Altogether, we have that the right hand side of eq. (21) is an approximation to the right hand side of eq. (18). In other words, the discrete energy E as defined in eq. (20) mimics the behavior of the continuous energy \mathcal{E} in eq. (18).

Moreover, similar to the 1D case, the free surface boundary condition can also be imposed by appending penalty terms to eq. (19). Taking the two xy -faces at $z = z_L$ and $z = z_R$ for example, the free surface boundary condition states that $\sigma_{xz} = \sigma_{yz} = \sigma_{zz} = 0$. These conditions can be imposed by modifying the updating formulas for the velocity components in eq. (19) as follows:

$$\left\{ \begin{array}{l} \mathcal{A}^{V_x} \boldsymbol{\rho}^{V_x} \frac{dV_x}{dt} = \mathcal{A}^{V_x} \left(\mathcal{D}_x^{\Sigma_{xx}} \Sigma_{xx} + \mathcal{D}_y^{\Sigma_{xy}} \Sigma_{xy} + \mathcal{D}_z^{\Sigma_{xz}} \Sigma_{xz} \right) \\ \quad + (\mathcal{I}_x^M \otimes \mathcal{I}_y^N \otimes \mathcal{E}_z^L) \cdot (\mathcal{A}_x^M \otimes \mathcal{A}_y^N) \cdot \left[(\mathcal{I}_x^M \otimes \mathcal{I}_y^N \otimes \mathcal{P}_z^L)^T \Sigma_{xz} - \mathbf{0} \right] \\ \quad - (\mathcal{I}_x^M \otimes \mathcal{I}_y^N \otimes \mathcal{E}_z^R) \cdot (\mathcal{A}_x^M \otimes \mathcal{A}_y^N) \cdot \left[(\mathcal{I}_x^M \otimes \mathcal{I}_y^N \otimes \mathcal{P}_z^R)^T \Sigma_{xz} - \mathbf{0} \right]; \\ \mathcal{A}^{V_y} \boldsymbol{\rho}^{V_y} \frac{dV_y}{dt} = \mathcal{A}^{V_y} \left(\mathcal{D}_x^{\Sigma_{xy}} \Sigma_{xy} + \mathcal{D}_y^{\Sigma_{yy}} \Sigma_{yy} + \mathcal{D}_z^{\Sigma_{yz}} \Sigma_{yz} \right) \\ \quad + (\mathcal{I}_x^N \otimes \mathcal{I}_y^M \otimes \mathcal{E}_z^L) \cdot (\mathcal{A}_x^N \otimes \mathcal{A}_y^M) \cdot \left[(\mathcal{I}_x^N \otimes \mathcal{I}_y^M \otimes \mathcal{P}_z^L)^T \Sigma_{yz} - \mathbf{0} \right] \\ \quad - (\mathcal{I}_x^N \otimes \mathcal{I}_y^M \otimes \mathcal{E}_z^R) \cdot (\mathcal{A}_x^N \otimes \mathcal{A}_y^M) \cdot \left[(\mathcal{I}_x^N \otimes \mathcal{I}_y^M \otimes \mathcal{P}_z^R)^T \Sigma_{yz} - \mathbf{0} \right]; \\ \mathcal{A}^{V_z} \boldsymbol{\rho}^{V_z} \frac{dV_z}{dt} = \mathcal{A}^{V_z} \left(\mathcal{D}_x^{\Sigma_{xz}} \Sigma_{xz} + \mathcal{D}_y^{\Sigma_{yz}} \Sigma_{yz} + \mathcal{D}_z^{\Sigma_{zz}} \Sigma_{zz} \right) \\ \quad + (\mathcal{I}_x^N \otimes \mathcal{I}_y^N \otimes \mathcal{P}_z^L) \cdot (\mathcal{A}_x^N \otimes \mathcal{A}_y^N) \cdot \left[(\mathcal{I}_x^N \otimes \mathcal{I}_y^N \otimes \mathcal{E}_z^L)^T \Sigma_{zz} - \mathbf{0} \right] \\ \quad - (\mathcal{I}_x^N \otimes \mathcal{I}_y^N \otimes \mathcal{P}_z^R) \cdot (\mathcal{A}_x^N \otimes \mathcal{A}_y^N) \cdot \left[(\mathcal{I}_x^N \otimes \mathcal{I}_y^N \otimes \mathcal{E}_z^R)^T \Sigma_{zz} - \mathbf{0} \right], \end{array} \right. \quad (23a)$$

$$\left. \begin{array}{l} \mathcal{A}^{V_y} \boldsymbol{\rho}^{V_y} \frac{dV_y}{dt} = \mathcal{A}^{V_y} \left(\mathcal{D}_x^{\Sigma_{xy}} \Sigma_{xy} + \mathcal{D}_y^{\Sigma_{yy}} \Sigma_{yy} + \mathcal{D}_z^{\Sigma_{yz}} \Sigma_{yz} \right) \\ \quad + (\mathcal{I}_x^N \otimes \mathcal{I}_y^M \otimes \mathcal{E}_z^L) \cdot (\mathcal{A}_x^N \otimes \mathcal{A}_y^M) \cdot \left[(\mathcal{I}_x^N \otimes \mathcal{I}_y^M \otimes \mathcal{P}_z^L)^T \Sigma_{yz} - \mathbf{0} \right] \\ \quad - (\mathcal{I}_x^N \otimes \mathcal{I}_y^M \otimes \mathcal{E}_z^R) \cdot (\mathcal{A}_x^N \otimes \mathcal{A}_y^M) \cdot \left[(\mathcal{I}_x^N \otimes \mathcal{I}_y^M \otimes \mathcal{P}_z^R)^T \Sigma_{yz} - \mathbf{0} \right]; \end{array} \right. \quad (23b)$$

$$\left. \begin{array}{l} \mathcal{A}^{V_z} \boldsymbol{\rho}^{V_z} \frac{dV_z}{dt} = \mathcal{A}^{V_z} \left(\mathcal{D}_x^{\Sigma_{xz}} \Sigma_{xz} + \mathcal{D}_y^{\Sigma_{yz}} \Sigma_{yz} + \mathcal{D}_z^{\Sigma_{zz}} \Sigma_{zz} \right) \\ \quad + (\mathcal{I}_x^N \otimes \mathcal{I}_y^N \otimes \mathcal{P}_z^L) \cdot (\mathcal{A}_x^N \otimes \mathcal{A}_y^N) \cdot \left[(\mathcal{I}_x^N \otimes \mathcal{I}_y^N \otimes \mathcal{E}_z^L)^T \Sigma_{zz} - \mathbf{0} \right] \\ \quad - (\mathcal{I}_x^N \otimes \mathcal{I}_y^N \otimes \mathcal{P}_z^R) \cdot (\mathcal{A}_x^N \otimes \mathcal{A}_y^N) \cdot \left[(\mathcal{I}_x^N \otimes \mathcal{I}_y^N \otimes \mathcal{E}_z^R)^T \Sigma_{zz} - \mathbf{0} \right], \end{array} \right. \quad (23c)$$

where the penalty terms appended to eqs. (23a), (23b), and (23c) correspond to conditions $\sigma_{xz} = 0$, $\sigma_{yz} = 0$, and $\sigma_{zz} = 0$, respectively. It can be verified that the penalty terms introduced above would cancel out the last six lines in eq. (21) (i.e., those included in the last bracket that corresponds to the xy -faces) in discrete energy analysis.

We note here that appending penalty terms to the discretized system can be viewed as modifying the corresponding spatial derivative approximations. This realization will help simplify the upcoming discussion. For example, appending the penalty terms in eqs. (23a), (23b), and (23c) can be viewed as replacing $\mathcal{D}_z^{\Sigma_{xz}} \Sigma_{xz}$, $\mathcal{D}_z^{\Sigma_{yz}} \Sigma_{yz}$, and $\mathcal{D}_z^{\Sigma_{zz}} \Sigma_{zz}$, respectively,

with their modified spatial derivative approximations defined as follows:

$$\begin{aligned} \overline{\mathcal{D}_z^{\Sigma_{xz}} \Sigma_{xz}} &= \mathcal{D}_z^{\Sigma_{xz}} \Sigma_{xz} + \left\{ \mathcal{I}_x^M \otimes \mathcal{I}_y^N \otimes \left[(\mathcal{A}_z^N)^{-1} \mathcal{E}_z^L \right] \right\} \cdot \left[(\mathcal{I}_x^M \otimes \mathcal{I}_y^N \otimes \mathcal{P}_z^L)^T \Sigma_{xz} - \mathbf{0} \right] \\ &\quad - \left\{ \mathcal{I}_x^M \otimes \mathcal{I}_y^N \otimes \left[(\mathcal{A}_z^N)^{-1} \mathcal{E}_z^R \right] \right\} \cdot \left[(\mathcal{I}_x^M \otimes \mathcal{I}_y^N \otimes \mathcal{P}_z^R)^T \Sigma_{xz} - \mathbf{0} \right]; \end{aligned} \quad (24a)$$

$$\begin{aligned} \overline{\mathcal{D}_z^{\Sigma_{yz}} \Sigma_{yz}} &= \mathcal{D}_z^{\Sigma_{yz}} \Sigma_{yz} + \left\{ \mathcal{I}_x^N \otimes \mathcal{I}_y^M \otimes \left[(\mathcal{A}_z^N)^{-1} \mathcal{E}_z^L \right] \right\} \cdot \left[(\mathcal{I}_x^N \otimes \mathcal{I}_y^M \otimes \mathcal{P}_z^L)^T \Sigma_{yz} - \mathbf{0} \right] \\ &\quad - \left\{ \mathcal{I}_x^N \otimes \mathcal{I}_y^M \otimes \left[(\mathcal{A}_z^N)^{-1} \mathcal{E}_z^R \right] \right\} \cdot \left[(\mathcal{I}_x^N \otimes \mathcal{I}_y^M \otimes \mathcal{P}_z^R)^T \Sigma_{yz} - \mathbf{0} \right]; \end{aligned} \quad (24b)$$

$$\begin{aligned} \overline{\mathcal{D}_z^{\Sigma_{zz}} \Sigma_{zz}} &= \mathcal{D}_z^{\Sigma_{zz}} \Sigma_{zz} + \left\{ \mathcal{I}_x^N \otimes \mathcal{I}_y^N \otimes \left[(\mathcal{A}_z^M)^{-1} \mathcal{P}_z^L \right] \right\} \cdot \left[(\mathcal{I}_x^N \otimes \mathcal{I}_y^N \otimes \mathcal{E}_z^L)^T \Sigma_{zz} - \mathbf{0} \right] \\ &\quad - \left\{ \mathcal{I}_x^N \otimes \mathcal{I}_y^N \otimes \left[(\mathcal{A}_z^M)^{-1} \mathcal{P}_z^R \right] \right\} \cdot \left[(\mathcal{I}_x^N \otimes \mathcal{I}_y^N \otimes \mathcal{E}_z^R)^T \Sigma_{zz} - \mathbf{0} \right], \end{aligned} \quad (24c)$$

where inverses of the norm matrices \mathcal{A}^{V_x} , \mathcal{A}^{V_y} , and \mathcal{A}^{V_z} have been applied to the penalty terms in eqs. (23a), (23b), and (23c), respectively. Using the modified spatial derivative approximations introduced above, the norm matrices \mathcal{A}^{V_x} , \mathcal{A}^{V_y} , and \mathcal{A}^{V_z} can now be omitted from the discretized system, though their impact remains through the modified spatial derivative approximations.

3.3 Interface conditions and interpolation operators

At the interface between two neighboring layers, we seek to impose the following interface conditions (see, e.g., Stein & Wysesession 2009, p. 52):

$$\begin{cases} v_i^+ = v_i^-; & (25a) \\ \sigma_{ij}^+ n_j^+ + \sigma_{ij}^- n_j^- = 0, & (25b) \end{cases}$$

where symbols $^+$ and $^-$ are appended to distinguish quantities from the plus and minus sides of the interface. Eq. (25a) stems from continuity of the elastic medium, i.e., no overlap or tear, while eq. (25b) stems from Newton's third law. For the discretization setting considered in this work, where the layer interfaces are horizontal, the outward normal vectors n^+ and n^- in eq. (25) are simply $[0, 0, -1]^T$ and $[0, 0, 1]^T$, respectively, and the interface conditions in eq. (25) reduce to continuity in solution variables v_x , v_y , v_z , σ_{xz} , σ_{yz} , and σ_{zz} , with the remaining solution variables uninvolved.

These interface conditions can also be imposed by appending proper penalty terms to the discretized system described in eq. (19). Effectively, this boils down to modifying the spatial derivative approximations as in eqs. (26) and (27).

(On the plus side:)

$$\mathcal{D}_z^{\Sigma_{xz}^+} \Sigma_{xz}^+ \longrightarrow \overline{\mathcal{D}_z^{\Sigma_{xz}^+} \Sigma_{xz}^+} = \mathcal{D}_z^{\Sigma_{xz}^+} \Sigma_{xz}^+ + \frac{1}{2} \left\{ \mathcal{I}_{x^+}^M \otimes \mathcal{I}_{y^+}^N \otimes \left[(\mathcal{A}_{z^+}^N)^{-1} \mathcal{E}_{z^+}^L \right] \right\} \quad (26a)$$

$$\cdot \left\{ (\mathcal{I}_{x^+}^M \otimes \mathcal{I}_{y^+}^N \otimes \mathcal{P}_{z^+}^L)^T \Sigma_{xz}^+ - \mathcal{T}^{\Sigma_{xz}^-} \left[(\mathcal{I}_{x^-}^M \otimes \mathcal{I}_{y^-}^N \otimes \mathcal{P}_{z^-}^R)^T \Sigma_{xz}^- \right] \right\};$$

$$\mathcal{D}_z^{V_x^+} V_x^+ \longrightarrow \overline{\mathcal{D}_z^{V_x^+} V_x^+} = \mathcal{D}_z^{V_x^+} V_x^+ + \frac{1}{2} \left\{ \mathcal{I}_{x^+}^M \otimes \mathcal{I}_{y^+}^N \otimes \left[(\mathcal{A}_{z^+}^M)^{-1} \mathcal{P}_{z^+}^L \right] \right\} \quad (26b)$$

$$\cdot \left\{ (\mathcal{I}_{x^+}^M \otimes \mathcal{I}_{y^+}^N \otimes \mathcal{E}_{z^+}^L)^T V_x^+ - \mathcal{T}^{V_x^-} \left[(\mathcal{I}_{x^-}^M \otimes \mathcal{I}_{y^-}^N \otimes \mathcal{E}_{z^-}^R)^T V_x^- \right] \right\};$$

$$\mathcal{D}_z^{\Sigma_{yz}^+} \Sigma_{yz}^+ \longrightarrow \overline{\mathcal{D}_z^{\Sigma_{yz}^+} \Sigma_{yz}^+} = \mathcal{D}_z^{\Sigma_{yz}^+} \Sigma_{yz}^+ + \frac{1}{2} \left\{ \mathcal{I}_{x^+}^N \otimes \mathcal{I}_{y^+}^M \otimes \left[(\mathcal{A}_{z^+}^N)^{-1} \mathcal{E}_{z^+}^L \right] \right\} \quad (26c)$$

$$\cdot \left\{ (\mathcal{I}_{x^+}^N \otimes \mathcal{I}_{y^+}^M \otimes \mathcal{P}_{z^+}^L)^T \Sigma_{yz}^+ - \mathcal{T}^{\Sigma_{yz}^-} \left[(\mathcal{I}_{x^-}^N \otimes \mathcal{I}_{y^-}^M \otimes \mathcal{P}_{z^-}^R)^T \Sigma_{yz}^- \right] \right\};$$

$$\mathcal{D}_z^{V_y^+} V_y^+ \longrightarrow \overline{\mathcal{D}_z^{V_y^+} V_y^+} = \mathcal{D}_z^{V_y^+} V_y^+ + \frac{1}{2} \left\{ \mathcal{I}_{x^+}^N \otimes \mathcal{I}_{y^+}^M \otimes \left[(\mathcal{A}_{z^+}^M)^{-1} \mathcal{P}_{z^+}^L \right] \right\} \quad (26d)$$

$$\cdot \left\{ (\mathcal{I}_{x^+}^N \otimes \mathcal{I}_{y^+}^M \otimes \mathcal{E}_{z^+}^L)^T V_y^+ - \mathcal{T}^{V_y^-} \left[(\mathcal{I}_{x^-}^N \otimes \mathcal{I}_{y^-}^M \otimes \mathcal{E}_{z^-}^R)^T V_y^- \right] \right\};$$

$$\mathcal{D}_z^{\Sigma_{zz}^+} \Sigma_{zz}^+ \longrightarrow \overline{\mathcal{D}_z^{\Sigma_{zz}^+} \Sigma_{zz}^+} = \mathcal{D}_z^{\Sigma_{zz}^+} \Sigma_{zz}^+ + \frac{1}{2} \left\{ \mathcal{I}_{x^+}^N \otimes \mathcal{I}_{y^+}^N \otimes \left[(\mathcal{A}_{z^+}^M)^{-1} \mathcal{P}_{z^+}^L \right] \right\} \quad (26e)$$

$$\cdot \left\{ (\mathcal{I}_{x^+}^N \otimes \mathcal{I}_{y^+}^N \otimes \mathcal{E}_{z^+}^L)^T \Sigma_{zz}^+ - \mathcal{T}^{\Sigma_{zz}^-} \left[(\mathcal{I}_{x^-}^N \otimes \mathcal{I}_{y^-}^N \otimes \mathcal{E}_{z^-}^R)^T \Sigma_{zz}^- \right] \right\};$$

$$\mathcal{D}_z^{V_z^+} V_z^+ \longrightarrow \overline{\mathcal{D}_z^{V_z^+} V_z^+} = \mathcal{D}_z^{V_z^+} V_z^+ + \frac{1}{2} \left\{ \mathcal{I}_{x^+}^N \otimes \mathcal{I}_{y^+}^N \otimes \left[(\mathcal{A}_{z^+}^N)^{-1} \mathcal{E}_{z^+}^L \right] \right\} \quad (26f)$$

$$\cdot \left\{ (\mathcal{I}_{x^+}^N \otimes \mathcal{I}_{y^+}^N \otimes \mathcal{P}_{z^+}^L)^T V_z^+ - \mathcal{T}^{V_z^-} \left[(\mathcal{I}_{x^-}^N \otimes \mathcal{I}_{y^-}^N \otimes \mathcal{P}_{z^-}^R)^T V_z^- \right] \right\}.$$

(On the minus side:)

$$\mathcal{D}_z^{\Sigma_{xz}^-} \Sigma_{xz}^- \longrightarrow \overline{\mathcal{D}_z^{\Sigma_{xz}^-} \Sigma_{xz}^-} = \mathcal{D}_z^{\Sigma_{xz}^-} \Sigma_{xz}^- - \frac{1}{2} \left\{ \mathcal{I}_{x^-}^M \otimes \mathcal{I}_{y^-}^N \otimes \left[(\mathcal{A}_{z^-}^N)^{-1} \mathcal{E}_{z^-}^R \right] \right\} \quad (27a)$$

$$\cdot \left\{ (\mathcal{I}_{x^-}^M \otimes \mathcal{I}_{y^-}^N \otimes \mathcal{P}_{z^-}^R)^T \Sigma_{xz}^- - \mathcal{T}^{\Sigma_{xz}^+} \left[(\mathcal{I}_{x^+}^M \otimes \mathcal{I}_{y^+}^N \otimes \mathcal{P}_{z^+}^L)^T \Sigma_{xz}^+ \right] \right\};$$

$$\mathcal{D}_z^{V_x^-} V_x^- \longrightarrow \overline{\mathcal{D}_z^{V_x^-} V_x^-} = \mathcal{D}_z^{V_x^-} V_x^- - \frac{1}{2} \left\{ \mathcal{I}_{x^-}^M \otimes \mathcal{I}_{y^-}^N \otimes \left[(\mathcal{A}_{z^-}^M)^{-1} \mathcal{P}_{z^-}^R \right] \right\} \quad (27b)$$

$$\cdot \left\{ (\mathcal{I}_{x^-}^M \otimes \mathcal{I}_{y^-}^N \otimes \mathcal{E}_{z^-}^R)^T V_x^- - \mathcal{T}^{V_x^+} \left[(\mathcal{I}_{x^+}^M \otimes \mathcal{I}_{y^+}^N \otimes \mathcal{E}_{z^+}^L)^T V_x^+ \right] \right\};$$

$$\mathcal{D}_z^{\Sigma_{yz}^-} \Sigma_{yz}^- \longrightarrow \overline{\mathcal{D}_z^{\Sigma_{yz}^-} \Sigma_{yz}^-} = \mathcal{D}_z^{\Sigma_{yz}^-} \Sigma_{yz}^- - \frac{1}{2} \left\{ \mathcal{I}_{x^-}^N \otimes \mathcal{I}_{y^-}^M \otimes \left[(\mathcal{A}_{z^-}^N)^{-1} \mathcal{E}_{z^-}^R \right] \right\} \quad (27c)$$

$$\cdot \left\{ (\mathcal{I}_{x^-}^N \otimes \mathcal{I}_{y^-}^M \otimes \mathcal{P}_{z^-}^R)^T \Sigma_{yz}^- - \mathcal{T}^{\Sigma_{yz}^+} \left[(\mathcal{I}_{x^+}^N \otimes \mathcal{I}_{y^+}^M \otimes \mathcal{P}_{z^+}^L)^T \Sigma_{yz}^+ \right] \right\};$$

$$\mathcal{D}_z^{V_y^-} V_y^- \longrightarrow \overline{\mathcal{D}_z^{V_y^-} V_y^-} = \mathcal{D}_z^{V_y^-} V_y^- - \frac{1}{2} \left\{ \mathcal{I}_{x^-}^N \otimes \mathcal{I}_{y^-}^M \otimes \left[(\mathcal{A}_{z^-}^M)^{-1} \mathcal{P}_{z^-}^R \right] \right\} \quad (27d)$$

$$\cdot \left\{ (\mathcal{I}_{x^-}^N \otimes \mathcal{I}_{y^-}^M \otimes \mathcal{E}_{z^-}^R)^T V_y^- - \mathcal{T}^{V_y^+} \left[(\mathcal{I}_{x^+}^N \otimes \mathcal{I}_{y^+}^M \otimes \mathcal{E}_{z^+}^L)^T V_y^+ \right] \right\};$$

$$\mathcal{D}_z^{\Sigma_{zz}^-} \Sigma_{zz}^- \longrightarrow \overline{\mathcal{D}_z^{\Sigma_{zz}^-} \Sigma_{zz}^-} = \mathcal{D}_z^{\Sigma_{zz}^-} \Sigma_{zz}^- - \frac{1}{2} \left\{ \mathcal{I}_{x^-}^N \otimes \mathcal{I}_{y^-}^N \otimes \left[(\mathcal{A}_{z^-}^M)^{-1} \mathcal{P}_{z^-}^R \right] \right\} \quad (27e)$$

$$\cdot \left\{ (\mathcal{I}_{x^-}^N \otimes \mathcal{I}_{y^-}^N \otimes \mathcal{E}_{z^-}^R)^T \Sigma_{zz}^- - \mathcal{T}^{\Sigma_{zz}^+} \left[(\mathcal{I}_{x^+}^N \otimes \mathcal{I}_{y^+}^N \otimes \mathcal{E}_{z^+}^L)^T \Sigma_{zz}^+ \right] \right\};$$

$$\mathcal{D}_z^{V_z^-} V_z^- \longrightarrow \overline{\mathcal{D}_z^{V_z^-} V_z^-} = \mathcal{D}_z^{V_z^-} V_z^- - \frac{1}{2} \left\{ \mathcal{I}_{x^-}^N \otimes \mathcal{I}_{y^-}^N \otimes \left[(\mathcal{A}_{z^-}^N)^{-1} \mathcal{E}_{z^-}^R \right] \right\} \quad (27f)$$

$$\cdot \left\{ (\mathcal{I}_{x^-}^N \otimes \mathcal{I}_{y^-}^N \otimes \mathcal{P}_{z^-}^R)^T V_z^- - \mathcal{T}^{V_z^+} \left[(\mathcal{I}_{x^+}^N \otimes \mathcal{I}_{y^+}^N \otimes \mathcal{P}_{z^+}^L)^T V_z^+ \right] \right\}.$$

In eqs. (26) and (27), the continuity in σ_{xz} , v_x , σ_{yz} , v_y , σ_{zz} , and v_z are accounted for by eqs. (26a)-(26f) on the plus side, respectively, and by eqs. (27a)-(27f) on the minus side, respectively. Moreover, we use \mathcal{T} to denote a 2D interpolation operator acting on the inter-

face. For example, $\mathcal{T}^{V_z^+}$ in eq. (27f) operates on the projection of V_z^+ on the interface, i.e., $(\mathcal{I}_{x^+}^N \otimes \mathcal{I}_{y^+}^N \otimes \mathcal{P}_{z^+}^L)^T V_z^+$, providing the approximations to v_z at locations matching those of the projection of V_z^- on the interface, i.e., $(\mathcal{I}_{x^-}^N \otimes \mathcal{I}_{y^-}^N \otimes \mathcal{P}_{z^-}^R)^T V_z^-$.

The 2D interpolation operators appearing in eqs. (26) and (27) are constructed as tensor products of 1D interpolation operators as follows:

$$\begin{aligned} \mathcal{T}^{\Sigma_{xz}^+} &= \mathcal{T}^{V_{x^+}} = \mathcal{T}_{x^+}^M \otimes \mathcal{T}_{y^+}^N, & \mathcal{T}^{\Sigma_{xz}^-} &= \mathcal{T}^{V_{x^-}} = \mathcal{T}_{x^-}^M \otimes \mathcal{T}_{y^-}^N; \\ \mathcal{T}^{\Sigma_{yz}^+} &= \mathcal{T}^{V_{y^+}} = \mathcal{T}_{x^+}^N \otimes \mathcal{T}_{y^+}^M, & \mathcal{T}^{\Sigma_{yz}^-} &= \mathcal{T}^{V_{y^-}} = \mathcal{T}_{x^-}^N \otimes \mathcal{T}_{y^-}^M; \\ \mathcal{T}^{\Sigma_{zz}^+} &= \mathcal{T}^{V_{z^+}} = \mathcal{T}_{x^+}^N \otimes \mathcal{T}_{y^+}^N, & \mathcal{T}^{\Sigma_{zz}^-} &= \mathcal{T}^{V_{z^-}} = \mathcal{T}_{x^-}^N \otimes \mathcal{T}_{y^-}^N. \end{aligned} \quad (28)$$

To properly handle the nonconforming interface, the 1D building blocks in eq. (28) are required to satisfy the following properties:

$$\begin{aligned} \mathcal{A}_{x^+}^N \mathcal{T}_{x^-}^N &= (\mathcal{A}_{x^-}^N \mathcal{T}_{x^+}^N)^T, & \mathcal{A}_{x^+}^M \mathcal{T}_{x^-}^M &= (\mathcal{A}_{x^-}^M \mathcal{T}_{x^+}^M)^T; \\ \mathcal{A}_{y^+}^N \mathcal{T}_{y^-}^N &= (\mathcal{A}_{y^-}^N \mathcal{T}_{y^+}^N)^T, & \mathcal{A}_{y^+}^M \mathcal{T}_{y^-}^M &= (\mathcal{A}_{y^-}^M \mathcal{T}_{y^+}^M)^T. \end{aligned} \quad (29)$$

A collection of 1D interpolation operators satisfying the properties in eq. (29) are presented in Appendix B, corresponding to a variety of grid spacing ratios. Such ratios are allowed to be fractional numbers, instead of merely integers, which improves the application flexibility of the proposed discretization setting. Similar to the construction of SBP operators, these interpolation operators are also constructed with the assistance from symbolic computing software.

If the discrete energy analysis is carried out without regard to the interface conditions, it can be shown that the remaining terms associated with the interface are:

$$\begin{aligned} \frac{dE}{dt} &= - \left[\begin{aligned} & \left[(\Sigma_{xz}^+)^T (\mathcal{I}_{x^+}^M \otimes \mathcal{I}_{y^+}^N \otimes \mathcal{P}_{z^+}^L) \right] \cdot \left[\mathcal{A}_{x^+}^M \otimes \mathcal{A}_{y^+}^N \right] \cdot \left[(\mathcal{I}_{x^+}^M \otimes \mathcal{I}_{y^+}^N \otimes \mathcal{E}_{z^+}^L)^T V_{x^+} \right] \\ & - \left[(\Sigma_{yz}^+)^T (\mathcal{I}_{x^+}^N \otimes \mathcal{I}_{y^+}^M \otimes \mathcal{P}_{z^+}^L) \right] \cdot \left[\mathcal{A}_{x^+}^N \otimes \mathcal{A}_{y^+}^M \right] \cdot \left[(\mathcal{I}_{x^+}^N \otimes \mathcal{I}_{y^+}^M \otimes \mathcal{E}_{z^+}^L)^T V_{y^+} \right] \\ & - \left[(\Sigma_{zz}^+)^T (\mathcal{I}_{x^+}^N \otimes \mathcal{I}_{y^+}^N \otimes \mathcal{E}_{z^+}^L) \right] \cdot \left[\mathcal{A}_{x^+}^N \otimes \mathcal{A}_{y^+}^N \right] \cdot \left[(\mathcal{I}_{x^+}^N \otimes \mathcal{I}_{y^+}^N \otimes \mathcal{P}_{z^+}^L)^T V_{z^+} \right] \end{aligned} \right] \left. \vphantom{\frac{dE}{dt}} \right\} (+ \text{ side}) \\ &+ \left[\begin{aligned} & \left[(\Sigma_{xz}^-)^T (\mathcal{I}_{x^-}^M \otimes \mathcal{I}_{y^-}^N \otimes \mathcal{P}_{z^-}^R) \right] \cdot \left[\mathcal{A}_{x^-}^M \otimes \mathcal{A}_{y^-}^N \right] \cdot \left[(\mathcal{I}_{x^-}^M \otimes \mathcal{I}_{y^-}^N \otimes \mathcal{E}_{z^-}^L)^T V_{x^-} \right] \\ & + \left[(\Sigma_{yz}^-)^T (\mathcal{I}_{x^-}^N \otimes \mathcal{I}_{y^-}^M \otimes \mathcal{P}_{z^-}^R) \right] \cdot \left[\mathcal{A}_{x^-}^N \otimes \mathcal{A}_{y^-}^M \right] \cdot \left[(\mathcal{I}_{x^-}^N \otimes \mathcal{I}_{y^-}^M \otimes \mathcal{E}_{z^-}^L)^T V_{y^-} \right] \\ & + \left[(\Sigma_{zz}^-)^T (\mathcal{I}_{x^-}^N \otimes \mathcal{I}_{y^-}^N \otimes \mathcal{E}_{z^-}^R) \right] \cdot \left[\mathcal{A}_{x^-}^N \otimes \mathcal{A}_{y^-}^N \right] \cdot \left[(\mathcal{I}_{x^-}^N \otimes \mathcal{I}_{y^-}^N \otimes \mathcal{P}_{z^-}^L)^T V_{z^-} \right] \end{aligned} \right] \left. \vphantom{\frac{dE}{dt}} \right\} (- \text{ side}) \end{aligned} \quad (30)$$

Instead, carrying out the discrete energy analysis with the modifications presented in eqs. (26)-(27) and the properties in eq. (29), it can be shown that the remaining terms in eq. (30) are

cancelled out without introducing any extra term, i.e., the energy-conserving property is preserved across the interface.

To illustrate, let us consider the pairs $\{\Sigma_{zz}^+; V_z^+\}$ and $\{\Sigma_{zz}^-; V_z^-\}$ as an example. The remaining terms in eq. (30) associated with these pairs are at the third and the sixth lines, respectively. Now, carrying out the discrete energy analysis with the modified spatial derivative approximations presented in eqs. (26e), (26f), (27e), and (27f), the remaining terms in $\frac{dE}{dt}$ associated with these pairs become

$$- \frac{\left[(\Sigma_{zz}^+)^T (\mathcal{I}_{x^+}^N \otimes \mathcal{I}_{y^+}^N \otimes \mathcal{E}_{z^+}^L) \right] \cdot \left[\mathcal{A}_{x^+}^N \otimes \mathcal{A}_{y^+}^N \right] \cdot \left[(\mathcal{I}_{x^+}^N \otimes \mathcal{I}_{y^+}^N \otimes \mathcal{P}_{z^+}^L)^T V_z^+ \right]}{\quad} \quad (31a)$$

$$+ \frac{\left[(\Sigma_{zz}^-)^T (\mathcal{I}_{x^-}^N \otimes \mathcal{I}_{y^-}^N \otimes \mathcal{E}_{z^-}^L) \right] \cdot \left[\mathcal{A}_{x^-}^N \otimes \mathcal{A}_{y^-}^N \right] \cdot \left[(\mathcal{I}_{x^-}^N \otimes \mathcal{I}_{y^-}^N \otimes \mathcal{P}_{z^-}^L)^T V_z^- \right]}{\quad} \quad (31b)$$

$$+ \frac{1}{2} \frac{\left[(V_z^+)^T (\mathcal{I}_{x^+}^N \otimes \mathcal{I}_{y^+}^N \otimes \mathcal{P}_{z^+}^L) \right] \cdot \left[\mathcal{A}_{x^+}^N \otimes \mathcal{A}_{y^+}^N \right] \cdot \left[(\mathcal{I}_{x^+}^N \otimes \mathcal{I}_{y^+}^N \otimes \mathcal{E}_{z^+}^L)^T \Sigma_{zz}^+ \right]}{\quad} \quad (31c)$$

$$- \frac{1}{2} \frac{\left[(V_z^+)^T (\mathcal{I}_{x^+}^N \otimes \mathcal{I}_{y^+}^N \otimes \mathcal{P}_{z^+}^L) \right] \cdot \left[(\mathcal{A}_{x^+}^N \mathcal{T}_{x^+}^N) \otimes (\mathcal{A}_{y^+}^N \mathcal{T}_{y^+}^N) \right] \cdot \left[(\mathcal{I}_{x^-}^N \otimes \mathcal{I}_{y^-}^N \otimes \mathcal{E}_{z^-}^L)^T \Sigma_{zz}^- \right]}{\quad} \quad (31d)$$

$$+ \frac{1}{2} \frac{\left[(\Sigma_{zz}^+)^T (\mathcal{I}_{x^+}^N \otimes \mathcal{I}_{y^+}^N \otimes \mathcal{E}_{z^+}^L) \right] \cdot \left[\mathcal{A}_{x^+}^N \otimes \mathcal{A}_{y^+}^N \right] \cdot \left[(\mathcal{I}_{x^+}^N \otimes \mathcal{I}_{y^+}^N \otimes \mathcal{P}_{z^+}^L)^T V_z^+ \right]}{\quad} \quad (31e)$$

$$- \frac{1}{2} \frac{\left[(\Sigma_{zz}^+)^T (\mathcal{I}_{x^+}^N \otimes \mathcal{I}_{y^+}^N \otimes \mathcal{E}_{z^+}^L) \right] \cdot \left[(\mathcal{A}_{x^+}^N \mathcal{T}_{x^+}^N) \otimes (\mathcal{A}_{y^+}^N \mathcal{T}_{y^+}^N) \right] \cdot \left[(\mathcal{I}_{x^-}^N \otimes \mathcal{I}_{y^-}^N \otimes \mathcal{P}_{z^-}^L)^T V_z^- \right]}{\quad} \quad (31f)$$

$$- \frac{1}{2} \frac{\left[(V_z^-)^T (\mathcal{I}_{x^-}^N \otimes \mathcal{I}_{y^-}^N \otimes \mathcal{P}_{z^-}^L) \right] \cdot \left[\mathcal{A}_{x^-}^N \otimes \mathcal{A}_{y^-}^N \right] \cdot \left[(\mathcal{I}_{x^-}^N \otimes \mathcal{I}_{y^-}^N \otimes \mathcal{E}_{z^-}^L)^T \Sigma_{zz}^- \right]}{\quad} \quad (31g)$$

$$+ \frac{1}{2} \frac{\left[(V_z^-)^T (\mathcal{I}_{x^-}^N \otimes \mathcal{I}_{y^-}^N \otimes \mathcal{P}_{z^-}^L) \right] \cdot \left[(\mathcal{A}_{x^-}^N \mathcal{T}_{x^-}^N) \otimes (\mathcal{A}_{y^-}^N \mathcal{T}_{y^-}^N) \right] \cdot \left[(\mathcal{I}_{x^+}^N \otimes \mathcal{I}_{y^+}^N \otimes \mathcal{E}_{z^+}^L)^T \Sigma_{zz}^+ \right]}{\quad} \quad (31h)$$

$$- \frac{1}{2} \frac{\left[(\Sigma_{zz}^-)^T (\mathcal{I}_{x^-}^N \otimes \mathcal{I}_{y^-}^N \otimes \mathcal{E}_{z^-}^L) \right] \cdot \left[\mathcal{A}_{x^-}^N \otimes \mathcal{A}_{y^-}^N \right] \cdot \left[(\mathcal{I}_{x^-}^N \otimes \mathcal{I}_{y^-}^N \otimes \mathcal{P}_{z^-}^L)^T V_z^- \right]}{\quad} \quad (31i)$$

$$+ \frac{1}{2} \frac{\left[(\Sigma_{zz}^-)^T (\mathcal{I}_{x^-}^N \otimes \mathcal{I}_{y^-}^N \otimes \mathcal{E}_{z^-}^L) \right] \cdot \left[(\mathcal{A}_{x^-}^N \mathcal{T}_{x^-}^N) \otimes (\mathcal{A}_{y^-}^N \mathcal{T}_{y^-}^N) \right] \cdot \left[(\mathcal{I}_{x^+}^N \otimes \mathcal{I}_{y^+}^N \otimes \mathcal{P}_{z^+}^L)^T V_z^+ \right]}{\quad}, \quad (31j)$$

where eqs. (31a) and (31b) are the third and the sixth lines of eq. (30), respectively; eqs. (31c) and (31d) stem from the modification in eq. (26e); eqs. (31e) and (31f) stem from the modification in eq. (26f); eqs. (31g) and (31h) stem from the modification in eq. (27e); eqs. (31i) and (31j) stem from the modification in eq. (27f). It can be verified easily that in eq. (31), terms underlined with lines of the same style cancel out. The properties from eq. (29) are needed for the terms underlined with the dashed and dotted lines to cancel out, respectively.

To sum up, all remaining terms in eq. (30) associated with the pairs $\{\Sigma_{zz}^+; V_z^+\}$ and $\{\Sigma_{zz}^-; V_z^-\}$ are cancelled out without introducing new terms because of the modifications made in eqs. (26e), (26f), (27e), and (27f). Similar observations can be made for the pairs $\{\Sigma_{xz}^+; V_x^+\}$ and $\{\Sigma_{xz}^-; V_x^-\}$, which correspond to the first and fourth lines of eq. (30), respectively, and for the pairs $\{\Sigma_{yz}^+; V_y^+\}$ and $\{\Sigma_{yz}^-; V_y^-\}$, which correspond to the second and fifth lines of eq. (30), respectively.

4 NUMERICAL EXAMPLES

In this section, two numerical examples are presented to corroborate the above analytical development, one concerning a layer-wise homogeneous model while the other concerning the overthrust model (Aminzadeh et al. 1997). To demonstrate the energy-conserving property, periodic boundary conditions are considered for the two horizontal directions (i.e., the x - and y -directions) while free surface boundary conditions are considered for the top and bottom boundaries as there is no energy loss associated with these boundary conditions. The periodic boundary conditions are addressed using the standard practice of wrapping the stencils around the boundaries. The staggered leapfrog scheme is used for temporal discretization.

4.1 Layered model

In this example, we consider a model consisting of four homogeneous layers. The relevant physical and numerical parameters associated with these layers (from top to bottom) are displayed in Table 1.

Table 1: Physical and numerical parameters associated with the layered model.

	c_s	c_p	ρ	Δx	N_{ppw}
Layer 1	300 m/s	800 m/s	1600 kg/m ³	1 m	12
Layer 2	600 m/s	1800 m/s	2100 kg/m ³	2 m	12
Layer 3	900 m/s	2400 m/s	2300 kg/m ³	3 m	12
Layer 4	2700 m/s	5000 m/s	2500 kg/m ³	9 m	12

The source profile is specified as the Ricker wavelet with central frequency at 10 Hz. The maximal frequency in the wave content is counted as 25 Hz, which is used to calculate the N_{ppw} (i.e., number of discretization grid points per minimal wavelength) shown in Table 1. The grid spacing ratios at the layer interfaces are 1:2, 2:3, and 1:3, respectively, from top to bottom. The temporal step size Δt is specified as $\sim 5.132E-04$ s, which corresponds to eq. (A.5) with $\mathbb{C}_{\text{CFL}} = 0.8$. For comparison, the uniform grid simulation with $\Delta x = 1$ for all layers is also performed. The temporal step size used in the uniform grid simulation is $\sim 9.2376E-05$ s, which corresponds to eq. (A.3) with $\mathbb{C}_{\text{CFL}} = 0.8$. (We note here that the maximal constant \mathbb{C}_{CFL} associated with the interior stencil $[^{1/24}, -^{9/8}, ^{9/8}, -^{1/24}]/\Delta x$ is $6/7 \approx 0.857$; see Levander (1988).) Between the two simulations, the ratio of spatial discretization points is ~ 3.438 ; the ratio of temporal discretization points is ~ 5.556 ; the ratio of total spatial-temporal discretization points is ~ 19.1 .

The size of the simulation domain is $1080 \text{ m} \times 1080 \text{ m} \times 1080 \text{ m}$, with the depth for each layer being 270 m . A compressional source is applied on the normal stress components while the V_z component of the velocity is recorded for comparison. The source and receiver are placed at 540 m apart from each other on both the x - and y -directions, and at 5 m (i.e., 5 grid points) and 4.5 m (i.e., 4.5 grid points) below the top boundary, respectively.

The recorded seismograms are displayed in Fig. 4, where we observe satisfactory agreement between these two simulations. A further verification is presented in Fig. 5, where three times finer grid spacing is used in both simulations. Slightly improved agreement can be observed in Fig. 5. Moreover, evolutions of the discrete energy in both simulations are displayed in Fig. 6, which remain constant after the source term tapers off and hence corroborate the energy-conserving property. We note here that the first 0.5 s are omitted in Fig. 6, which is the period when the source terms take effect and inject energy to the simulations. Additionally, snapshots of the vertical cross sections of the wavefield (V_z component) at the middle of the x -direction are illustrated in Fig. 7 for both nonuniform (left) and uniform (right) simulations. These snapshots are produced with the sources placed in the center of the xy -plane, near the top surface, and taken at $\sim 0.739 \text{ s}$.

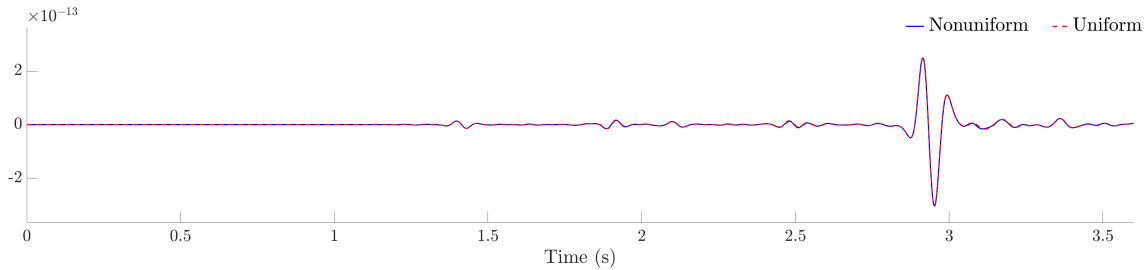


Figure 4: Recorded seismograms from nonuniform and uniform grid simulations.

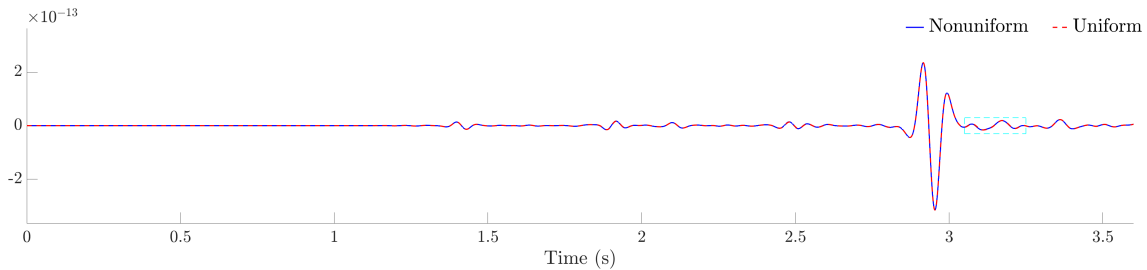


Figure 5: Recorded seismograms from nonuniform and uniform grid simulations. Grid spacings used in these simulations are three times finer than those used for Fig. 4. Slight improvement can be observed in the seismogram inside the cyan box.

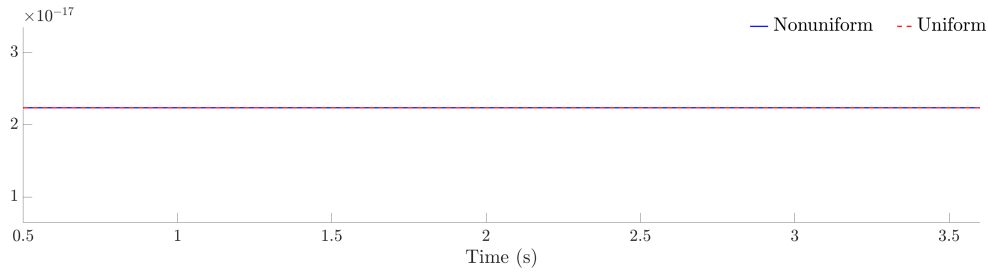


Figure 6: Evolution of the discrete energy in nonuniform and uniform grid simulations.



Figure 7: Snapshots of the vertical cross sections of the wavefield (V_z component) taken at the middle of the x -direction and ~ 0.739 s. Left: nonuniform simulation; Right: uniform simulation. These snapshots are produced with the sources placed in the center of the xy -plane, near the top surface.

4.2 Overthrust model

In this example, we test the proposed layer-wise discretization with the overthrust model, whose compressional wave speed is illustrated in Fig. 8. The model is described by $801 \times 801 \times 181$ parameter grid points. (For convenience, the last six grid points in the z -direction of the original model are omitted, which are inside the homogeneous zone in the bottom of the model.) Grid spacing between two neighboring parameter grid points is assigned to be 10 m here. Since the overthrust model contains only the information of the compressional wave speed c_p , we synthesize the shear wave speed c_s by prescribing the c_p/c_s ratio, which decreases from top (4.5) to bottom (1.5) linearly. (We note here that the c_p/c_s ratio tends to decrease with depth and increased degree of consolidation in rocks; see Gregory (1976);

Hamilton (1979).) Moreover, the density ρ is also synthesized, which increases from top (2000 kg/m³) to bottom (2700 kg/m³) linearly.

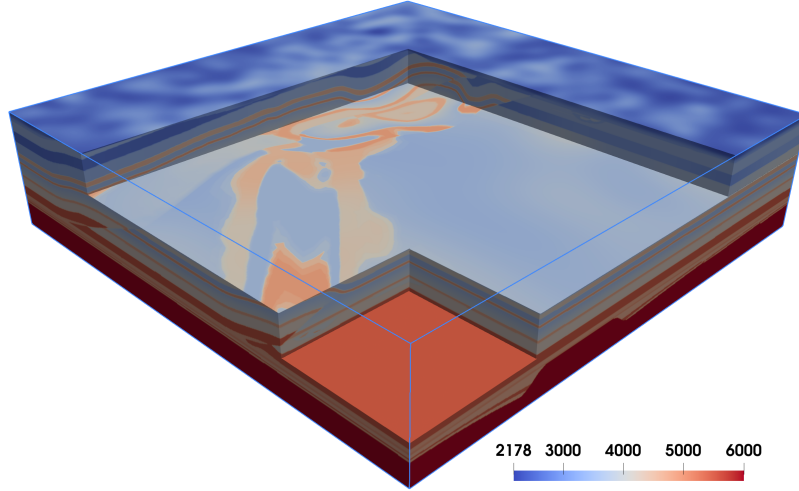


Figure 8: Compressional wave speed of the overthrust model. Portions of the model are carved out to illustrate the internal structures. Colorbar represents value of the compressional wave speed in unit m/s.

In nonuniform grid simulation, the entire simulation domain is separated into three layers of equal depth (600 m). The most relevant physical and numerical parameters associated with these layers are displayed in Table 2. The source profile is specified as the Ricker wavelet with central frequency at 5 Hz. The maximal frequency in the wave content is counted as 12.5 Hz, which is used to calculate the N_{ppw} shown in Table 2. The grid spacing ratios at both layer interfaces are 1:2. The temporal step size Δt is specified as $\sim 2.3072E-04$ s, which corresponds to eq. (A.5) with $\mathbb{C}_{\text{CFL}} = 0.8$. For comparison, the uniform grid simulation with $\Delta x = 2.5$ for all layers is also performed. The temporal step size used in the uniform grid simulation is $\sim 1.9245E-04$ s, which corresponds to eq. (A.3) with $\mathbb{C}_{\text{CFL}} = 0.8$. Between the two simulations, the ratio of spatial discretization points is ~ 2.63 ; the ratio of temporal discretization points is ~ 1.2 ; the ratio of total spatial-temporal discretization points is ~ 3.153 .

Table 2: Physical and numerical parameters associated with the layered model.

	min. c_s	max. c_p	Δx	N_{ppw}
Layer 1	~ 484.2 m/s	~ 5004.7 m/s	2.5 m	~ 15.5
Layer 2	958.5 m/s	5500 m/s	5 m	~ 15.3
Layer 3	1920 m/s	6000 m/s	10 m	~ 15.4

In terms of physical units, the size of the simulation domain is $8000 \text{ m} \times 8000 \text{ m} \times 1800 \text{ m}$. A compressional source is applied on the normal stress components while the V_z component of the velocity is recorded for comparison. The source and receiver are placed at 4000 m apart from each other on both the x - and y -directions, and at 12.5 m (i.e., 5 grid points) and 11.25 m (i.e., 4.5 grid points) below the top boundary, respectively.

The recorded seismograms are displayed in Fig. 9, where we observe satisfactory agreement between these two simulations. Moreover, evolutions of the discrete energy in both simulations are displayed in Fig. 10, which remain constant after the source term tapers off and hence corroborate the energy-conserving property.

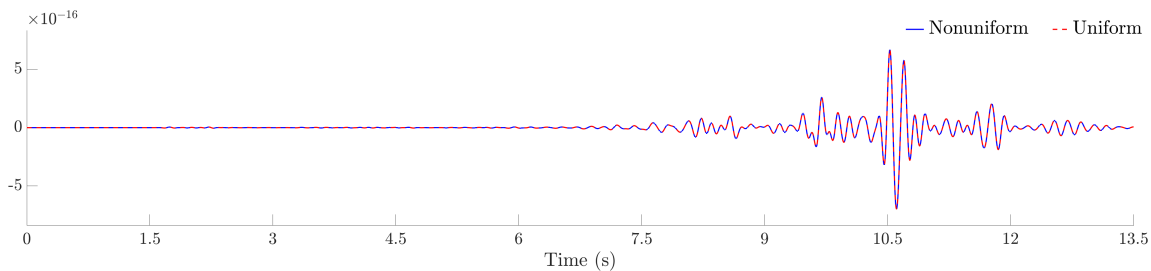


Figure 9: Recorded seismograms from nonuniform and uniform grid simulations.

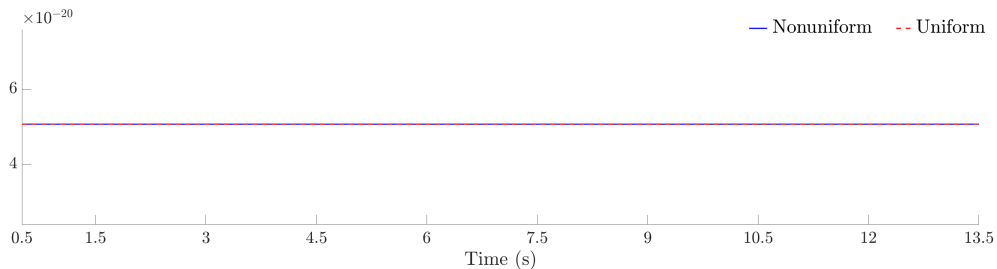


Figure 10: Evolution of the discrete energy in nonuniform and uniform grid simulations.

5 CONCLUSIONS

Finite difference discretization of the 3D isotropic elastic wave propagation on layer-wise uniform staggered grids with nonconforming interfaces has been considered in this work. It has been demonstrated that energy-conserving simulation across the nonconforming layer interfaces can be achieved through the usage of summation-by-parts finite difference operators, simultaneous approximation terms, and compatible interpolation operators, which ensures the stability of the simulation. Moreover, by examining the process of determining discretization parameters for seismic wave simulations under the standard constraints, as presented in

Appendix A, and by the numerical examples illustrated in Section 4, it has been shown that, compared to applying finite difference discretization on holistically uniform grids, significant reduction of computational resources can be achieved by employing the proposed layer-wise uniform discretization configuration.

REFERENCES

- Aminzadeh, F., Jean, B., & Kunz, T., 1997. *3-D salt and overthrust models*, Society of Exploration Geophysicists.
- Bao, H., Bielak, J., Ghattas, O., Kallivokas, L. F., O’Hallaron, D. R., Shewchuk, J. R., & Xu, J., 1998. Large-scale simulation of elastic wave propagation in heterogeneous media on parallel computers, *Computer Methods in Applied Mechanics and Engineering*, **152**(1–2), 85–102.
- Bourbié, T., Coussy, O., & Zinszner, B., 1987. *Acoustics of Porous Media*, Institut Français du Pétrole Publications, Editions Technip.
- Bui-Thanh, T. & Ghattas, O., 2012. Analysis of an hp-nonconforming discontinuous Galerkin spectral element method for wave propagation, *SIAM Journal on Numerical Analysis*, **50**(3), 1801–1826.
- Carpenter, M., Gottlieb, D., & Abarbanel, S., 1994. Time-stable boundary conditions for finite-difference schemes solving hyperbolic systems: methodology and application to high-order compact schemes, *Journal of Computational Physics*, **111**(2), 220–236.
- Chaljub, E., Capdeville, Y., & Vilotte, J.-P., 2003. Solving elastodynamics in a fluid–solid heterogeneous sphere: a parallel spectral element approximation on non-conforming grids, *Journal of Computational Physics*, **187**(2), 457–491.
- Chaljub, E., Komatitsch, D., Vilotte, J.-P., Capdeville, Y., Valette, B., & Festa, G., 2007. Spectral-element analysis in seismology, *Advances in geophysics*, **48**, 365–419.
- Dumbser, M. & Käser, M., 2006. An arbitrary high-order discontinuous Galerkin method for elastic waves on unstructured meshes – II. The three-dimensional isotropic case, *Geophysical Journal International*, **167**(1), 319–336.
- Etienne, V., Chaljub, E., Virieux, J., & Glinsky, N., 2010. An hp-adaptive discontinuous Galerkin finite-element method for 3-D elastic wave modelling, *Geophysical Journal International*, **183**(2), 941–962.
- Fernández, D., Hicken, J., & Zingg, D., 2014. Review of summation-by-parts operators with simultaneous approximation terms for the numerical solution of partial differential equations, *Computers & Fluids*, **95**, 171–196.
- Gao, L. & Keyes, D., 2019. Combining finite element and finite difference methods for isotropic elastic wave simulations in an energy-conserving manner, *Journal of Computational Physics*, **378**, 665–685.
- Gao, L. & Keyes, D., 2020a. Explicit coupling of acoustic and elastic wave propagation in finite-difference simulations, *GEOPHYSICS*, **85**(5), T293–T308.

- Gao, L. & Keyes, D., 2020b. Simultaneous approximation terms for elastic wave equations on nonuniform grids, in *Domain Decomposition Methods in Science and Engineering XXV*, pp. 125–133, Springer International Publishing.
- Gao, L., Ketcheson, D., & Keyes, D., 2018. On long-time instabilities in staggered finite difference simulations of the seismic acoustic wave equations on discontinuous grids, *Geophysical Journal International*, **212**(2), 1098–1110.
- Gao, L., Fernández, D., Carpenter, M., & Keyes, D., 2019. SBP-SAT finite difference discretization of acoustic wave equations on staggered block-wise uniform grids, *Journal of Computational and Applied Mathematics*, **348**, 421–444.
- Gregory, A., 1976. Fluid saturation effects on dynamic elastic properties of sedimentary rocks, *Geophysics*, **41**(5), 895–921.
- Hamilton, E. L., 1979. v_p/v_s and Poisson’s ratios in marine sediments and rocks, *The Journal of the Acoustical Society of America*, **66**(4), 1093–1101.
- Hayashi, K., Burns, D. R., & Toksöz, M. N., 2001. Discontinuous-grid finite-difference seismic modeling including surface topography, *Bulletin of the Seismological Society of America*, **91**(6), 1750–1764.
- Hesthaven, J. & Warburton, T., 2008. *Nodal discontinuous Galerkin methods: algorithms, analysis, and applications*, Springer Science & Business Media.
- Hicken, J. & Zingg, D., 2013. Summation-by-parts operators and high-order quadrature, *Journal of Computational and Applied Mathematics*, **237**(1), 111–125.
- Käser, M. & Dumbser, M., 2006. An arbitrary high-order discontinuous Galerkin method for elastic waves on unstructured meshes – I. The two-dimensional isotropic case with external source terms, *Geophysical Journal International*, **166**(2), 855–877.
- Komatitsch, D. & Tromp, J., 1999. Introduction to the spectral element method for three-dimensional seismic wave propagation, *Geophysical Journal International*, **139**(3), 806–822.
- Komatitsch, D. & Tromp, J., 2002. Spectral-element simulations of global seismic wave propagation – I. Validation, *Geophysical Journal International*, **149**(2), 390–412.
- Komatitsch, D. & Vilotte, J.-P., 1998. The spectral element method: An efficient tool to simulate the seismic response of 2D and 3D geological structures, *Bulletin of the Seismological Society of America*, **88**(2), 368–392.
- Kozdon, J. & Wilcox, L., 2016. Stable coupling of nonconforming, high-order finite difference methods, *SIAM Journal on Scientific Computing*, **38**(2), A923–A952.
- Kreiss, H.-O. & Scherer, G., 1974. *Finite element and finite difference methods for hyperbolic partial differential equations*. In: *Mathematical aspects of finite elements in partial differential equations*, Academic Press.
- Kristek, J., Moczo, P., & Galis, M., 2010. Stable discontinuous staggered grid in the finite-difference modelling of seismic motion, *Geophysical Journal International*, **183**(3), 1401–1407.
- Levander, A., 1988. Fourth-order finite-difference P-SV seismograms, *Geophysics*, **53**(11), 1425–1436.

- Lysmer, J. & Drake, L. A., 1972. A finite element method for seismology, in *Methods in Computational Physics: Advances in Research and Applications*, vol. 11, pp. 181–216, Academic Press.
- Mattsson, K. & O’Reilly, O., 2018. Compatible diagonal-norm staggered and upwind sbp operators, *Journal of Computational Physics*, **352**, 52 – 75.
- Nie, S., Wang, Y., Olsen, K. B., & Day, S. M., 2017. Fourth-order staggered-grid finite-difference seismic wavefield estimation using a discontinuous mesh interface (WEDMI), *Bulletin of the Seismological Society of America*, **107**(5), 2183–2193.
- O’Reilly, O., Lundquist, T., Dunham, E. M., & Nordström, J., 2017. Energy stable and high-order-accurate finite difference methods on staggered grids, *Journal of Computational Physics*, **346**, 572–589.
- Peter, D., Komatitsch, D., Luo, Y., Martin, R., Le Goff, N., Casarotti, E., Le Loher, P., Magnoni, F., Liu, Q., Blitz, C., Nissen-Meyer, T., Basini, P., & Tromp, J., 2011. Forward and adjoint simulations of seismic wave propagation on fully unstructured hexahedral meshes, *Geophysical Journal International*, **186**(2), 721–739.
- Prochnow, B., O’Reilly, O., Dunham, E., & Petersson, N., 2017. Treatment of the polar coordinate singularity in axisymmetric wave propagation using high-order summation-by-parts operators on a staggered grid, *Computers & Fluids*, **149**, 138–149.
- Stein, S. & Wysession, M., 2009. *An introduction to seismology, earthquakes, and earth structure*, John Wiley & Sons.
- Strand, B., 1994. Summation by parts for finite difference approximations for d/dx , *Journal of Computational Physics*, **110**(1), 47–67.
- Svärd, M. & Nordström, J., 2014. Review of summation-by-parts schemes for initial–boundary-value problems, *Journal of Computational Physics*, **268**, 17–38.
- Virieux, J., 1986. P-SV wave propagation in heterogeneous media: Velocity-stress finite-difference method, *Geophysics*, **51**(4), 889–901.
- Wang, S., Virta, K., & Kreiss, G., 2016. High order finite difference methods for the wave equation with non-conforming grid interfaces, *Journal of Scientific Computing*, **68**(3), 1002–1028.
- Wilcox, L. C., Stadler, G., Burstedde, C., & Ghattas, O., 2010. A high-order discontinuous Galerkin method for wave propagation through coupled elastic-acoustic media, *Journal of Computational Physics*, **229**(24), 9373–9396.
- Yee, K., 1966. Numerical solution of initial boundary value problems involving Maxwell’s equations in isotropic media, *IEEE Transactions on Antennas and Propagation*, **14**(3), 302–307.
- Zhang, Z., Zhang, W., Li, H., & Chen, X., 2013. Stable discontinuous grid implementation for collocated-grid finite-difference seismic wave modelling, *Geophysical Journal International*, **192**(3), 1179–1188.

Appendix A Impact of wave speed variation on discretization parameters

First, considering a uniformly discretized holistic simulation domain associated with a medium whose wave speed ranges from c_{\min} to c_{\max} , the minimal wavelength of the simulated waves can be expressed as

$$\lambda_{\min} = \frac{c_{\min}}{f}, \quad (\text{A.1})$$

where f denotes the highest frequency in the wave content being simulated. Assuming that the spatial grid spacing Δx is determined by prescribing N_{ppw} grid points to resolve the minimal wavelength λ_{\min} , we have that

$$\Delta x = \frac{\lambda_{\min}}{N_{\text{ppw}}} = \frac{c_{\min}}{f \cdot N_{\text{ppw}}}. \quad (\text{A.2})$$

Further assuming that the temporal step size Δt is determined by the CFL constraint, we can write

$$\Delta t = \mathbb{C}_{\text{CFL}} \cdot \frac{\Delta x}{c_{\max}} = \frac{\mathbb{C}_{\text{CFL}}}{f \cdot N_{\text{ppw}}} \cdot \frac{c_{\min}}{c_{\max}}, \quad (\text{A.3})$$

where \mathbb{C}_{CFL} is a constant that depends on the spatial and temporal discretization schemes, but independent of the underlying medium.

Regarding f , N_{ppw} , and \mathbb{C}_{CFL} as fixed constants in the above formulas, we observe from eq. (A.2) that the spatial grid spacing Δx is proportional to the minimal wave speed c_{\min} of the underlying medium; moreover, we observe from eq. (A.3) that the temporal step size Δt is constrained by the maximal contrast in the wave speed, i.e., c_{\max}/c_{\min} , of the underlying medium.

On the other hand, if the same simulation domain is separated into N_L layers, each discretized uniformly by prescribing N_{ppw} grid points to resolve the minimal wavelength within the layer, the spatial grid spacing for each layer can be expressed as

$$\Delta x^i = \frac{\lambda_{\min}^i}{N_{\text{ppw}}} = \frac{c_{\min}^i}{f \cdot N_{\text{ppw}}}, \quad i = 1 \cdots N_L, \quad (\text{A.4})$$

where Δx^i , λ_{\min}^i , and c_{\min}^i stand for the spatial grid spacing, minimal wavelength, and minimal wave speed of the i th layer. In other words, the spatial grid spacing is now only limited by the minimal wave speed within the layer, instead of the minimal wave speed of the entire simulation domain. Moreover, assuming that constant \mathbb{C}_{CFL} remains unchanged, the temporal step size is now determined by the most stringent CFL constraint among all layers, i.e.,

$$\Delta t = \mathbb{C}_{\text{CFL}} \cdot \min_{i=1 \cdots N_L} \left\{ \frac{\Delta x^i}{c_{\max}^i} \right\} = \frac{\mathbb{C}_{\text{CFL}}}{f \cdot N_{\text{ppw}}} \cdot \min_{i=1 \cdots N_L} \left\{ \frac{c_{\min}^i}{c_{\max}^i} \right\}, \quad (\text{A.5})$$

which is likely to be relaxed from, at least not worse than, that of eq. (A.3).

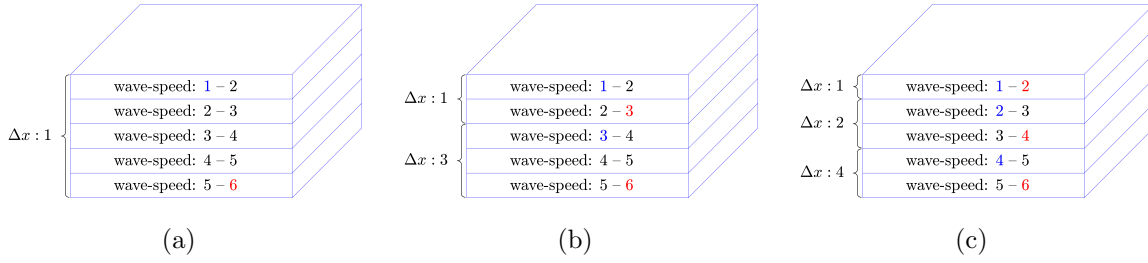


Figure A.1: A simple model to illustrate the potential benefit of layer-wise uniform discretization over holistically uniform discretization for wave simulations in earth media. The same simulation domain is considered in all three cases: in (a), the entire simulation domain is discretized uniformly; in (b), the entire simulation domain is separated into two layers, each discretized uniformly; in (c), the entire simulation domain is separated into three layers, each discretized uniformly. The normalized minimal and maximal wave speeds of each uniform discretization region are colored in blue and red, respectively; the former determines the spatial grid spacing Δx , while their ratio constrains the temporal step size Δt .

To give a concrete example, consider the simulation domain depicted in Fig. A.1, which consists of five regions of equal depth with progressively increasing wave speeds. The normalized minimal and maximal wave speeds of each region are displayed in the figure.

Fig. A.1(a) depicts the case that the entire simulation domain is discretized uniformly as a holistic region, which is used as the reference for comparison. The total number of its space-time discretization grid points is counted as

$$(1 + 1 + 1 + 1 + 1) \times 6 = 30 \text{ units}, \quad (\text{A.6})$$

where the quantity inside the parentheses corresponds to the total spatial discretization grid points, while the number 6 is related to the temporal discretization grid points, stemming from the maximal contrast in the wave speed of the entire simulation domain; see eq. (A.3).

Fig. A.1(b) depicts the case that the entire simulation domain is separated into two layers, each discretized uniformly and with a 1:3 ratio in Δx , the total number of space-time discretization grid points becomes

$$\left(1 + 1 + \frac{1}{27} + \frac{1}{27} + \frac{1}{27}\right) \times 3 \approx 6.3333 \text{ units}, \quad (\text{A.7})$$

where the number 3 stems from the maximal contrast in the wave speed of the top layer; see eq. (A.5). By comparing eq. (A.7) to eq. (A.6), we observe that the total number of space-time discretization grid points has been reduced by a factor of ~ 4.7 .

Fig. A.1(c) depicts the case that the entire simulation domain is separated into three layers, each discretized uniformly and with a 1:2:4 ratio in Δx , the total number of space-

time discretization grid points becomes

$$\left(1 + \frac{1}{8} + \frac{1}{8} + \frac{1}{64} + \frac{1}{64}\right) \times 2 = 2.5625 \text{ units}, \quad (\text{A.8})$$

where the number 2 stems from the maximal contrast in the wave speed of the top layer (or the middle layer); see eq. (A.5). By comparing eq. (A.8) to eq. (A.6), we observe that the total number of space-time discretization grid points has been reduced by a factor of ~ 11.7 .

We note here that for realistic earth media, it rarely happens that different layers can be separated in such a non-overlapping fashion as shown in Fig. A.1, where the maximal wave speed in one layer matches the minimal wave speed of the next. Instead, there are often overlaps in the wave speed ranges of two neighboring layers. In such a situation, the cost saving factors estimated above can be overly optimistic. On the other hand, instead of the equal-depth model considered in Fig. A.1, a relatively thin layer of low velocity surface material (e.g., sand and soil) often appears in realistic situations, which can severely restrict the choices of discretization parameters in holistically uniform simulations. In such cases, the actual cost saving factors can be more pronounced than those estimated above. Finally, addressing layer interfaces can incur computational overheads in simulations, which may also affect the actual cost saving factors. However, impact from such overheads tends to be insignificant for large simulations at realistic scales.

Appendix B Compatible interpolation operators

A collection of 1D interpolation operators for a variety of grid spacing ratios are presented in the following. They are the building blocks for the 2D interpolation operators used in Section 3.3 to address the nonconforming interfaces. These interpolation operators are referred to as being compatible (with each other), since, in addition to the typical approximation requirements, they also satisfy the reciprocal relationship postulated in eq. (29).

Because of this reciprocal relationship, only the interpolation operators from the coarse grid (minus side) to the fine grid (plus side) are presented since the interpolation operators for the opposite direction can be deduced based on eq. (29). Furthermore, only the formulas for a few exemplifying grid points within a repeating cycle are shown in the following, while formulas for the other grid points can be replicated by shifting the indices accordingly.

1:2 grid spacing ratio

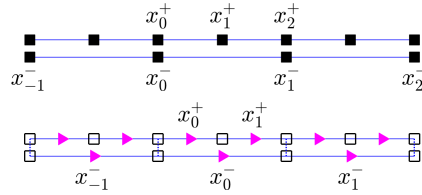


Figure B.1: Illustration of the grid points involved in formulas in eqs. (B.1) and (B.2) for interpolation operators $T_{x^-}^N$ (top) and $T_{x^-}^M$ (bottom). The grid spacing ratio is 1:2.

$T_{x^-}^N$:

$$\begin{aligned}
 f(x_0^+) &\leftarrow f(x_0^-) \\
 f(x_1^+) &\leftarrow -\frac{1}{16}f(x_{-1}^-) + \frac{9}{16}f(x_0^-) + \frac{9}{16}f(x_1^-) - \frac{1}{16}f(x_2^-) \\
 f(x_2^+) &\leftarrow f(x_1^-)
 \end{aligned} \tag{B.1}$$

$T_{x^-}^M$:

$$\begin{aligned}
 f(x_0^+) &\leftarrow \frac{5}{32}f(x_0^-) + \frac{15}{16}f(x_1^-) - \frac{3}{32}f(x_2^-) \\
 f(x_1^+) &\leftarrow -\frac{3}{32}f(x_0^-) + \frac{15}{16}f(x_1^-) + \frac{5}{32}f(x_2^-)
 \end{aligned} \tag{B.2}$$

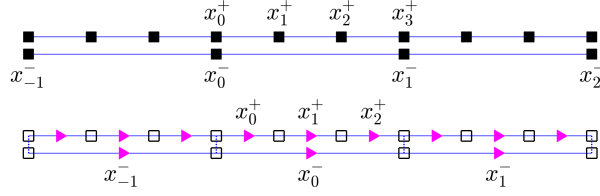
1:3 grid spacing ratio

Figure B.2: Illustration of the grid points involved in formulas in eqs. (B.3) and (B.4) for interpolation operators $T_{x^-}^N$ (top) and $T_{x^-}^M$ (bottom). The grid spacing ratio is 1:3.

$T_{x^-}^N$:

$$\begin{aligned}
 f(x_0^+) &\leftarrow f(x_0^-) \\
 f(x_1^+) &\leftarrow -\frac{1}{9}f(x_{-1}^-) + \frac{8}{9}f(x_0^-) + \frac{2}{9}f(x_1^-) \\
 f(x_2^+) &\leftarrow \frac{2}{9}f(x_0^-) + \frac{8}{9}f(x_1^-) - \frac{1}{9}f(x_2^-) \\
 f(x_3^+) &\leftarrow f(x_1^-)
 \end{aligned} \tag{B.3}$$

$T_{x^-}^M$:

$$\begin{aligned}
 f(x_0^+) &\leftarrow \frac{2}{9}f(x_{-1}^-) + \frac{8}{9}f(x_0^-) - \frac{1}{9}f(x_1^-) \\
 f(x_1^+) &\leftarrow f(x_0^-) \\
 f(x_2^+) &\leftarrow -\frac{1}{9}f(x_{-1}^-) + \frac{8}{9}f(x_0^-) + \frac{2}{9}f(x_1^-)
 \end{aligned} \tag{B.4}$$

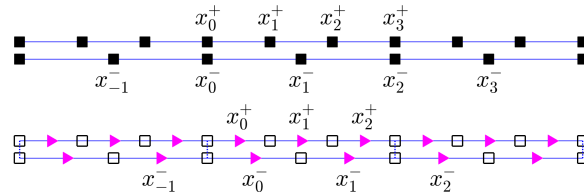
2:3 grid spacing ratio

Figure B.3: Illustration of the grid points involved in formulas in eqs. (B.5) and (B.6) for interpolation operators $T_{x^-}^N$ (top) and $T_{x^-}^M$ (bottom). The grid spacing ratio is 2:3.

$T_{x^-}^N$:

$$\begin{aligned}
 f(x_0^+) &\leftarrow f(x_0^-) \\
 f(x_1^+) &\leftarrow -\frac{11}{288}f(x_{-1}^-) + \frac{1}{3}f(x_0^-) + \frac{113}{144}f(x_1^-) - \frac{1}{12}f(x_2^-) + \frac{1}{288}f(x_3^-) \\
 f(x_2^+) &\leftarrow \frac{1}{288}f(x_{-1}^-) - \frac{1}{12}f(x_0^-) + \frac{113}{144}f(x_1^-) + \frac{1}{3}f(x_2^-) - \frac{11}{288}f(x_3^-) \\
 f(x_3^+) &\leftarrow f(x_2^-)
 \end{aligned} \tag{B.5}$$

$T_{x^-}^M :$

$$\begin{aligned}
 f(x_0^+) &\leftarrow \frac{101}{1152}f(x_{-1}^-) + \frac{1153}{1152}f(x_0^-) - \frac{113}{1152}f(x_1^-) + \frac{11}{1152}f(x_2^-) \\
 f(x_1^+) &\leftarrow -\frac{1}{16}f(x_{-1}^-) + \frac{9}{16}f(x_0^-) + \frac{9}{16}f(x_1^-) - \frac{1}{16}f(x_2^-) \\
 f(x_2^+) &\leftarrow \frac{11}{1152}f(x_{-1}^-) - \frac{113}{1152}f(x_0^-) + \frac{1153}{1152}f(x_1^-) + \frac{101}{1152}f(x_2^-)
 \end{aligned} \tag{B.6}$$

1:4 grid spacing ratio

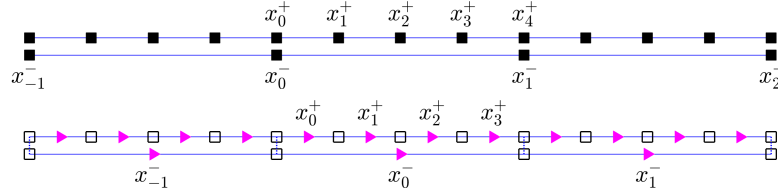


Figure B.4: Illustration of the grid points involved in formulas in eqs. (B.7) and (B.8) for interpolation operators $T_{x^-}^N$ (top) and $T_{x^-}^M$ (bottom). The grid spacing ratio is 1:4.

 $T_{x^-}^N :$

$$\begin{aligned}
 f(x_0^+) &\leftarrow f(x_0^-) \\
 f(x_1^+) &\leftarrow -\frac{3}{32}f(x_{-1}^-) + \frac{15}{16}f(x_0^-) + \frac{5}{32}f(x_1^-) \\
 f(x_2^+) &\leftarrow -\frac{1}{16}f(x_{-1}^-) + \frac{9}{16}f(x_0^-) + \frac{9}{16}f(x_1^-) - \frac{1}{16}f(x_2^-) \\
 f(x_3^+) &\leftarrow \frac{5}{32}f(x_0^-) + \frac{15}{16}f(x_1^-) - \frac{3}{32}f(x_2^-) \\
 f(x_4^+) &\leftarrow f(x_1^-)
 \end{aligned} \tag{B.7}$$

 $T_{x^-}^M :$

$$\begin{aligned}
 f(x_0^+) &\leftarrow \frac{33}{128}f(x_{-1}^-) + \frac{55}{64}f(x_0^-) - \frac{15}{128}f(x_1^-) \\
 f(x_1^+) &\leftarrow \frac{9}{128}f(x_{-1}^-) + \frac{63}{64}f(x_0^-) - \frac{7}{128}f(x_1^-) \\
 f(x_2^+) &\leftarrow -\frac{7}{128}f(x_{-1}^-) + \frac{63}{64}f(x_0^-) + \frac{9}{128}f(x_1^-) \\
 f(x_3^+) &\leftarrow -\frac{15}{128}f(x_{-1}^-) + \frac{55}{64}f(x_0^-) + \frac{33}{128}f(x_1^-)
 \end{aligned} \tag{B.8}$$

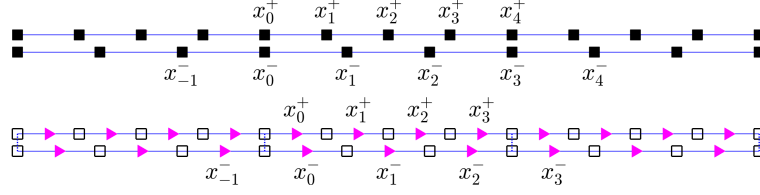
3:4 grid spacing ratio

Figure B.5: Illustration of the grid points involved in formulas in eqs. (B.9) and (B.10) for interpolation operators $T_{x^-}^N$ (top) and $T_{x^-}^M$ (bottom). The grid spacing ratio is 3:4.

$T_{x^-}^N$:

$$\begin{aligned}
 f(x_0^+) &\leftarrow f(x_0^-) \\
 f(x_1^+) &\leftarrow -\frac{119}{4320}f(x_{-1}^-) + \frac{67}{288}f(x_0^-) + \frac{629}{720}f(x_1^-) - \frac{367}{4320}f(x_2^-) + \frac{1}{160}f(x_3^-) \\
 f(x_2^+) &\leftarrow \frac{7}{2160}f(x_{-1}^-) - \frac{13}{180}f(x_0^-) + \frac{1229}{2160}f(x_1^-) + \frac{1229}{2160}f(x_2^-) - \frac{13}{180}f(x_3^-) + \frac{7}{2160}f(x_4^-) \\
 f(x_3^+) &\leftarrow \frac{1}{160}f(x_0^-) - \frac{367}{4320}f(x_1^-) + \frac{629}{720}f(x_2^-) + \frac{67}{288}f(x_3^-) - \frac{119}{4320}f(x_4^-) \\
 f(x_4^+) &\leftarrow f(x_3^-)
 \end{aligned} \tag{B.9}$$

$T_{x^-}^M$:

$$\begin{aligned}
 f(x_0^+) &\leftarrow \frac{35}{576}f(x_{-1}^-) + \frac{389}{384}f(x_0^-) - \frac{1}{12}f(x_1^-) + \frac{11}{1152}f(x_2^-) \\
 f(x_1^+) &\leftarrow -\frac{77}{1728}f(x_{-1}^-) + \frac{1325}{3456}f(x_0^-) + \frac{3}{4}f(x_1^-) - \frac{335}{3456}f(x_2^-) + \frac{7}{864}f(x_3^-) \\
 f(x_2^+) &\leftarrow \frac{7}{864}f(x_{-1}^-) - \frac{335}{3456}f(x_0^-) + \frac{3}{4}f(x_1^-) + \frac{1325}{3456}f(x_2^-) - \frac{77}{1728}f(x_3^-) \\
 f(x_3^+) &\leftarrow \frac{11}{1152}f(x_0^-) - \frac{1}{12}f(x_1^-) + \frac{389}{384}f(x_2^-) + \frac{35}{576}f(x_3^-)
 \end{aligned} \tag{B.10}$$

We note here that the above interpolation formulas are designed such that the leading error terms in the approximations are of at least third order. However, even under this condition, they are not the unique choice for compatible interpolation operators. Taking the 2:3 grid spacing ratio for example, the interpolation operators shown in eqs. (B.11) and (B.12) are also suitable choices.

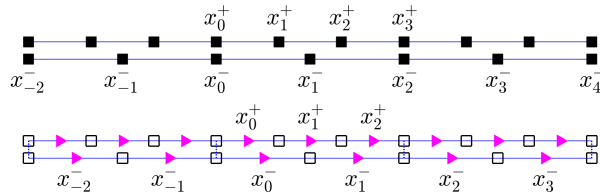


Figure B.6: Illustration of the grid points involved in formulas in eqs. (B.11) and (B.12) for interpolation operators $T_{x^-}^N$ (top) and $T_{x^-}^M$ (bottom). The grid spacing ratio is 2:3.

$T_{x^-}^N :$

$$\begin{aligned}
f(x_0^+) &\leftarrow -\frac{1}{96}f(x_{-2}^-) + \frac{1}{24}f(x_{-1}^-) + \frac{15}{16}f(x_0^-) + \frac{1}{24}f(x_1^-) - \frac{1}{96}f(x_2^-) \\
f(x_1^+) &\leftarrow -\frac{13}{288}f(x_{-1}^-) + \frac{103}{288}f(x_0^-) + \frac{217}{288}f(x_1^-) - \frac{19}{288}f(x_2^-) \\
f(x_2^+) &\leftarrow -\frac{19}{288}f(x_0^-) + \frac{217}{288}f(x_1^-) + \frac{103}{288}f(x_2^-) - \frac{13}{288}f(x_3^-) \\
f(x_3^+) &\leftarrow -\frac{1}{96}f(x_0^-) + \frac{1}{24}f(x_1^-) + \frac{15}{16}f(x_2^-) + \frac{1}{24}f(x_3^-) - \frac{1}{96}f(x_4^-)
\end{aligned}
\tag{B.11}$$

 $T_{x^-}^M :$

$$\begin{aligned}
f(x_0^+) &\leftarrow -\frac{11}{576}f(x_{-2}^-) + \frac{89}{576}f(x_{-1}^-) + \frac{527}{576}f(x_0^-) - \frac{29}{576}f(x_1^-) \\
f(x_1^+) &\leftarrow -\frac{1}{16}f(x_{-1}^-) + \frac{9}{16}f(x_0^-) + \frac{9}{16}f(x_1^-) - \frac{1}{16}f(x_2^-) \\
f(x_2^+) &\leftarrow -\frac{29}{576}f(x_0^-) + \frac{527}{576}f(x_1^-) + \frac{89}{576}f(x_2^-) - \frac{11}{576}f(x_3^-)
\end{aligned}
\tag{B.12}$$

Appendix C SBP finite difference operators

The following 1D SBP finite difference operators in eqs. (C.1) and (C.2) are used as the building blocks for the 3D SBP operators presented in Section 3.2. We note here that these operators correspond to the case of unit grid spacing, i.e., $\Delta x = 1$. For general cases, \mathcal{D}^N and \mathcal{D}^M need to be scaled by $1/\Delta x$ while \mathcal{A}^N and \mathcal{A}^M need to be scaled by Δx .

$$\mathcal{D}^N = \begin{bmatrix} \begin{array}{ccccc} -79/78 & 27/26 & -1/26 & 1/78 & 0 \\ 2/21 & -9/7 & 9/7 & -2/21 & 0 \\ 1/75 & 0 & -27/25 & 83/75 & -1/25 \end{array} \\ \begin{array}{cccc} & 1/24 & -9/8 & 9/8 & -1/24 \\ & & 1/24 & -9/8 & 9/8 & -1/24 \\ & & & \ddots & \ddots & \ddots & \ddots \\ & & & & 1/24 & -9/8 & 9/8 & -1/24 \\ & & & & & 1/24 & -9/8 & 9/8 & -1/24 \end{array} \\ \begin{array}{ccccc} 1/25 & -83/75 & 27/25 & 0 & -1/75 \\ 0 & 2/21 & -9/7 & 9/7 & -2/21 \\ 0 & -1/78 & 1/26 & -27/26 & 79/78 \end{array} \end{bmatrix}; \quad (\text{C.1a})$$

$$\mathcal{D}^M = \begin{bmatrix} \begin{array}{ccccc} -2 & 3 & -1 & 0 & 0 \\ -1 & 1 & 0 & 0 & 0 \\ 1/24 & -9/8 & 9/8 & -1/24 & 0 \\ -1/71 & 6/71 & -83/71 & 81/71 & -3/71 \end{array} \\ \begin{array}{cccc} & 1/24 & -9/8 & 9/8 & -1/24 \\ & & 1/24 & -9/8 & 9/8 & -1/24 \\ & & & \ddots & \ddots & \ddots & \ddots \\ & & & & 1/24 & -9/8 & 9/8 & -1/24 \\ & & & & & 1/24 & -9/8 & 9/8 & -1/24 \end{array} \\ \begin{array}{ccccc} 3/71 & -81/71 & 83/71 & -6/71 & 1/71 \\ 0 & 1/24 & -9/8 & 9/8 & -1/24 \\ 0 & 0 & 0 & -1 & 1 \\ 0 & 0 & 1 & -3 & 2 \end{array} \end{bmatrix}. \quad (\text{C.1b})$$

given by

$$\mathcal{E}^L = \begin{bmatrix} 1 \\ 0 \\ \vdots \\ 0 \end{bmatrix}, \quad \mathcal{E}^R = \begin{bmatrix} 0 \\ \vdots \\ 0 \\ 1 \end{bmatrix}, \quad \mathcal{P}^L = \begin{bmatrix} 15/8 \\ -5/4 \\ 3/8 \\ 0 \\ \vdots \\ 0 \end{bmatrix}, \quad \mathcal{P}^R = \begin{bmatrix} 0 \\ \vdots \\ 0 \\ 3/8 \\ -5/4 \\ 15/8 \end{bmatrix}, \quad (\text{C.4})$$

respectively.